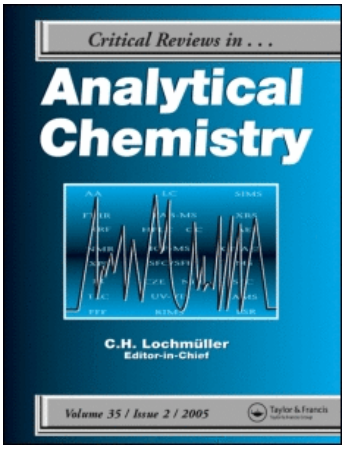

Critical Reviews in Analytical Chemistry
Publication details, including instructions for authors and subscription information:
http://www.informaworld.com/smpp/title~content=t713400837

Analysis of Chemical Data by Computer Modeling

James F. Rusling[a]
[a] Drexel University, Philadelphia, Pennsylvania

To cite this Article Rusling, James F.(1989) 'Analysis of Chemical Data by Computer Modeling', Critical Reviews in Analytical Chemistry, 21: 1, 49 — 81
To link to this Article: DOI: 10.1080/10408348908048816
URL: http://dx.doi.org/10.1080/10408348908048816

Analysis of Chemical Data by Computer Modeling

James F. Rusling

Referee: Louis Meites, Ph.D.
Department of Chemistry
George Mason University
Fairfax, Virginia

I. INTRODUCTION

The rapidly increasing power and availability of small computers have made sophisticated numerical analysis of data a routine feature of modern chemistry. Analytical computations that would have been too time consuming on a mainframe computer of 20 years ago have become commonplace on the laboratory microcomputers of today. On the other hand, some mainframe computer centers promise to offer "low-end supercomputing" by the early 1990s. This capability should further broaden the scope of feasible data analysis methods. Highly integrated measurement/computation systems are evolving concurrently with the ongoing revolution in computing technology partly because many instrumental measurements require mathematical treatment of raw data to make it more intelligible to the chemist. Data analysis packages are integral components of many modern commercial instruments used in chemistry. Mathematical operations may include transforming raw data into a more desirable form, removing unwanted instrumental background features, or extracting values of one or more physical or chemical parameters from the data.

Computer processing of instrumental data usually can be classified into one of two types. In the first, a mathematical procedure (often called an algorithm) is used to convert data into a more desirable form. Examples include derivatization of potentiometric titration curves to determine endpoints, integration of amperometric current vs. time curves to obtain chronocoulometric charge vs. time curves, and Fourier transformation to convert spectra from time to frequency domains. In the second type of processing, data are quantitatively analyzed with mathematical models of the expected behavior, resulting in validation of the correct model and evaluation of desired physical quantities as parameters of the model. Examples here include linear regression analysis of absorbance vs. concentration data to obtain the molar absorptivity of an analyte and nonlinear regression analysis of luminescence decay data to find lifetimes of photo-excited states. It is this second case, the analysis of chemical data with mathematical models, that forms the subject of this review. Specifically, I address usage and recent applications of nonlinear regression analysis for modeling chemical data.

A previous paper in the Critical Review series describing chemical applications of nonlinear regression analysis and extensions based on it was published in 1979 by Meites.[1] One stated purpose of that review was "to argue that nonlinear regression is such a powerful and versatile technique for handling chemical data that few chemists can afford the luxury of not using it."[1] With the rapid proliferation since 1979 of inexpensive and powerful microcomputers, this statement appears more valid than ever. However, the present review does not belabor previous arguments. It does, in the first few sections, provide a tutorial-style introduction to the use of nonlinear regression analysis (Section II) and the systematic building of models for experimental data (Section III). In Section IV, a series of illustrative examples of recent (since 1979) applications of nonlinear regression analysis in chemistry is presented. In the last section, the use of information contained in deviation plots obtained from nonlinear regression to construct computerized classification schemes, similar to what have lately become known as "expert systems", is discussed. This paper aims at familiarizing the reader with the techniques, the power, and the applicability of nonlinear regression analysis for solving a wide variety of chemical problems. It is not an exhaustive review; the applications discussed reflect mainly the author's research experience and interest.

II. FITTING MODELS TO DATA: NONLINEAR REGRESSION

A. Linear and Nonlinear Models

A "model" is the term used to describe an equation or set of equations which provide the ability to calculate a dependent variable (y), such as the response of an instrument, as a function of an independent variable (x) and a set of k + 1 physically meaningful parameters [B(i)]. The general mathematical form of such a model for j = 0 to n data points is then:

$$y_j(\text{calc}) = F\{x_j, B(0), B(1), \ldots, B(k)\} \quad (1)$$

While models with many independent variables are possible, here we are concerned mainly with the case of one independent variable. This is often called a "single-equation" model. Some examples of models with more than one independent variable are discussed in Section IV.F.

Regression analysis consists of simultaneous optimization of the parameters in the model with respect to a set of experimental data $[y_j(\text{meas}),x_j]$ so that the $y_j(\text{calc})$ computed from Equation 1 are as close as possible to the experimental

J. F. Rusling received his B.S. Chem. from Drexel University, Philadelphia, Pennsylvania; his Ph.D. was earned at Clarkson University, Potsdam, New York. Dr. Rusling is an Associate Professor in the Department of Chemistry, University of Connecticut, Storrs.

y_j(meas). This is called "fitting" the model to the data. It is usually done by using the principle of least squares, whereby the error sum, S,

$$S = \sum_{j=1}^{n} w_j[y_j(\text{meas}) - y_j(\text{calc})]^2 \quad (2)$$

is minimized with respect to the parameters. The w_j in Equation 2 are weighting factors. Their values depend on the relation of the standard error in y_j(meas) to the magnitude of the experimentally measured quantities. For example, when the random or standard error in y_j(meas) is independent of the size of y_j(meas), then all $w_j = 1$. This is discussed in more detail in Section II.C.

The simplest single-equation model is a straight line:

$$y_j(\text{calc}) = B(0)x_j + B(1) \quad (3)$$

Note that the dependent variable y_j(calc) is a *linear* function of the parameters B(0) and B(1). Thus, Equation 3 is called a linear model and can be fitted to the data by linear regression. This is effected by using exact formulas derived by setting the first derivative of the error sum S with respect to each parameter equal to zero and solving for the parameters. This yields a closed form equation for each parameter[1] giving the best estimates of slope B(0) and intercept B(1).

Linear regression is possible whenever the dependent variable y is a linear function of the parameters. Applicability of linear regression does not depend on a linear relation between y and x. (From now on, j subscripts are omitted in most places for the sake of simplicity.) However, experimental data often follow mathematical expressions depending on parameters in a nonlinear way. For example, if $y = B(0) + B(1)\log x$, y is a nonlinear function of x, but it is still linear with respect to the parameters B(0) and B(1), which can be determined by linear regression. On the other hand, in the equation describing the kinetics of first-order decay:

$$y = A'\exp[-kt] + B \quad (4)$$

Dependent variable y is a nonlinear function of the rate constant k. Here, t is time, A′ is the response at $t = 0$, and B represents a constant background signal. If $B = 0$, one option is to linearize Equation 4 by taking the logarithm of both sides:

$$\ln y = -kt + \ln A' \quad (5)$$

Linear regression onto Equation 5 can now be used, but ln y is the new dependent variable. The random error in ln y does not have the same relation to ln y as does the random error in y to the values of y. If random errors in y are independent of y, then errors in ln y *are not* independent of ln y. The use of $w_j = 1$ is not valid here[1] and weighted linear regression is required.

The situation is more complex when B is nonzero. If B is known, ln(y − B) can be made the dependent variable in a rearranged, linearized version of Equation 4. If B is not known, linearization presents a serious dilemma. A discussion of the hidden complexity of linearized equations and how they affect assumptions and procedures of linear regression has been presented.[1] Later in this review, a real example of unavoidable systematic error resulting from linearization is discussed. To be sure, an advantage of linear regression is its requirement of only one computing cycle. As we shall see, nonlinear regression requires a series of cycles which iteratively approach the correct answer. However, rapidly converging algorithms coupled with modern computing power allow most nonlinear regressions to be completed in minutes or seconds on microcomputers such as Apples, TRS-80s, or IBM/PCs.

Returning to the task of determining the parameters in Equation 4, nonlinear regression analysis is a fast, easy-to-use alternative to linearization. By employing it, the nonlinear Equation 4 can be fit directly to the experimental data by the least squares principle, giving the best values of the parameters A′, k, and B. The method is general and applicable to any model. It avoids creating a complex relation between y and its errors which might result from linearization of the model. Like linear regression, the nonlinear version seeks a minimum in an appropriate error sum, often the quantity S in Equation 2. Contrary to the linear regression, closed form equations for the best values of the parameters cannot be derived when y is a nonlinear function of one or more parameters. Thus, programs for nonlinear regression start from input "guesses" of the parameters and use an appropriate numerical algorithm to iteratively vary those parameters until the minimum in the error function is found. This so-called "convergence point" defines the best values of the parameters.

B. General Programs

Reliable computer programs utilizing various algorithms to minimize error sums are available for nonlinear regression. Two of these[2,3] are used routinely in our research group. There are many others. General programs have a "model subroutine" into which the user writes code describing the desired regression model. The model need not be an explicit closed form equation like Equation 4. It may be a series of equations, or any collection of mathematical expressions which supplies computed values of the dependent variable y_j(calc) to the main program. For example, as illustrated later in this review, numerical solutions of partial differential equations can be used to compute electrochemical current-potential curves[4-6] within nonlinear regression programs to obtain kinetic and thermodynamic parameters from voltammetric data.

The error sum S in Equation 2 with $w_j = 1$ is appropriate to minimize when standard errors in the measurements are independent of the magnitude of the y_j(meas). S is then called an unweighted error sum. The approach to minimum S starting from a set of arbitrary initial "best guesses" for k parameters

can be viewed as the journey of a point toward the minimum of an error surface in a k + 1 dimensional orthogonal coordinate system. (In practice, the coordidnates may not always be strictly orthogonal.) One axis of the coordinate system corresponds to the value of S and the others correspond to the parameter values. Suppose B = 0 in Equation 4. For the resulting two-parameter nonlinear regression, the error surface is three dimensional. The z-axis is associated with the error sum S, while the x- and y-axes are identified with the parameters A′ and k, respectively (Figure 1). From initial guesses of A'_i and k_i, an initial point P_i $[A_i,k_i,S_i]$ is located on the error surface. By systematic variation of the parameters, the algorithm employed by the program to minimize S causes this point to travel toward point P_o $[A'_o,k_o,S_o]$. This is the point of convergence, where S_o is at the absolute minimum on the error surface. The quantities A_o and k_o are the best values of the parameters, optimized with respect to the experimental data.

General programs for nonlinear regression differ mainly in the algorithm used to reach convergence. Since most users are interested mainly in applications, only a general picture of the workings of the most commonly used algorithms is given here. The program discussed in an earlier review[1] employs a modified steepest descent method. In such methods, the search for the minimum S travels on the gradient of the error surface. The progress of travel is monitored at each iteration or cycle and adjusted when necessary. Steepest descent provides rapid initial convergence, but it slows considerably near the convergence point. Such programs written with conservative tolerances for convergence have proved extremely reliable. The Gauss-Newton method, another frequently used algorithm, approximates the nonlinear expressions for y_j(calc) by linear Taylor's series expansions.[7,8] Then, following initial guesses, new values of

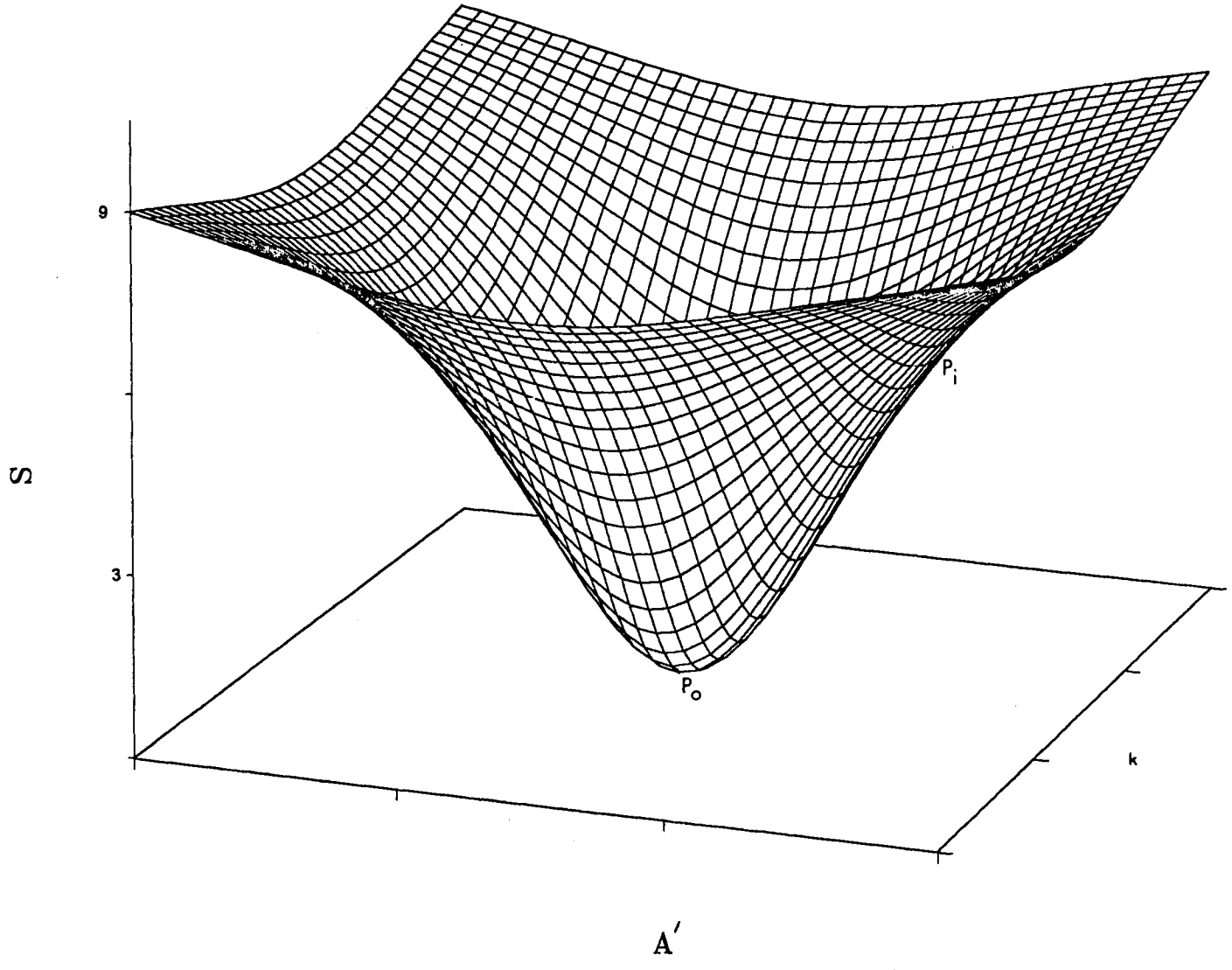

FIGURE 1. Conceptual graphical representation of an error surface for a two-parameter nonlinear regression analysis. Parameters are A′ and k.

the parameters at each cycle are found by methods similar to linear least squares, using expressions involving first derivatives of S with respect to each parameter. Ideally, each iterative cycle gives successively better estimates for the parameters until an absolute minimum in S is reached. Contrary to the steepest descent method, convergence is often fast in the vicinity of the minimum.

The Marquardt or Levenberg-Marquardt algorithm[8,9] contains elements of both steepest descent and Gauss-Newton methods. Operationally, the Marquardt algorithm behaves like a steepest descent method under conditions for which the latter is efficient, i.e., far from the minimum S. Close to the minimum, the Marquardt algorithm behaves like the Gauss-Newton method, again under conditions where the latter is efficient. In our hands, a program[3] based on the Marquardt algorithm has yielded excellent results, converging at essentially the same point and in many fewer cycles than steepest descent (or simplex) programs for the same problems. The Marquardt-based program in Reference 3 uses numerical differentiation so that analytical derivatives need not be provided by the user, as required in some Gauss-Newton programs. The only drawback noted has been a tendency to give matrix inversion errors[3] in some problems for certain values of the initial parameters. This has been alleviated somewhat by interfacing the program with a computer graphics subroutine which plots the experimental data along with the curve computed from the model. Thus, if initial guesses are very far off, it can immediately be seen and corrected. The regression is not started until initial guesses are considered to be reasonable by the user after inspecting the graph. Marquardt programs are often available in libraries of mainframe computer centers, e.g., in the Statistical Analysis System (SAS) package.

Another technique that can be used for nonlinear regression is the modified simplex method. For k parameters, this method involves a k + 1 dimensional geometric construct called a simplex. A three-dimensional simplex is a triangle. The algorithm is arranged such that the simplex simultaneously contracts in size and moves toward the minimum of the error surface. The method has been described in detail in the context of optimizing experimental parameters for maximum response in analytical methods.[10] Although our research group has not made extensive use of this technique, comparisons with steepest descent programs for three and four parameter regression analyses have demonstrated its reliability. Convergence times appear to be comparable to steepest descent methods, but longer than the Marquardt method.

Programs for nonlinear regression should include criteria to automatically test for convergence and terminate the program when preset conditions for convergence have been reached. Reliable tests for convergence are based on the rate of change of the parameters. For example, one program[2] commonly terminates when the rate of change of S over ten cycles is <0.02%. Another,[3] based on the Marquardt algorithm, converges normally when the change in all parameters in a given cycle is <0.005%. Criteria for convergence can often be adjusted by the user, but this is normally not necessary. In an algorithm as fast as the Levenberg-Marquardt, testing over a series of cycles is self-defeating in terms of computational time and does not appear to be necessary. Supplementary convergence criteria to handle special situations are provided in some programs.[2,3] Graphical evaluation of convergence by comparing computed and experimental data is generally less sensitive than the above methods. Although useful for rough evaluations of the model's validity, it is not recommended as an absolute test for convergence.

Before leaving the topic of convergence, a few words need to be said about so-called "false minima". The object of regression algorithms is to reach the absolute or global minimum of the error surface. If the surface is irregularly shaped, the algorithm could conceivably hang up in a local minimum or "well" with an error sum considerably larger than the global minimum. The parameter values would then be erroneous. Although such false minima are possible, in the experience of our research group for many, many, types of problems and thousands of sets of data, we have never encountered a local minimum in a well-conditioned, properly designed regression analysis. The use of computer graphics, mentioned above, also aids in avoiding starting points too far from the absolute minimum which might cause convergence to a false minimum. Local minima can be detected by beginning regression analyses with several different (but physically reasonable) sets of initial values of the parameters. Convergence to significantly different values of error sum and final parameters that depend strongly on the starting point of the computation suggests local minima. Convergence to identical values of error sum and parameters for any reasonable starting point suggests attainment of the global minimum.

C. What Error Sum to Minimize?

The relationship between random or standard errors in measuring dependent and independent variables and the measured values of these variables dictates the choice of the weighting factors w_j in the error sum (Equation 2) minimized in regression analyses. For a model with the general form of Equation 1, standard errors in both the dependent variable y and the independent variable x may be significant. However, a useful simplifying assumption is that standard error in x is negligible, i.e., the x_j are known with absolute precision. This is a commonly used assumption in linear and nonlinear regression analyses. It is probably accurate in many cases, such as when y is a slowly varying instrumental response measured vs. time as x. Time can often be measured much more accurately and precisely than many instrumental responses. Referring to Equation 4, suppose y is the measured variable at times between 10 and 5000 s. for an event with $t_{1/2}$ = 1000 s ($k = 6.93 \times 10^{-4}$ s^{-1}). Suppose a clock accurate to ±0.1 ms and a

spectrophotometer with an absolute standard error of ±0.001 A are used to make measurements between 0.01 and 0.20 A. Clearly, the standard error in y will be proportionally larger and much more significant than the error in x (i.e., time). Here, the assumption that errors in x are negligible is certainly valid. The error in t becomes important in determining k when it is $>0.005\ t_{1/2}$.[11]

If random errors in x can be neglected, only the random errors in y need be considered in the error sum. The next question to be addressed, then, is how does the standard error in y depend on the magnitude of y? If it is independent of y, or *absolute*, as in the example above, the error sum S in Equation 2 with $w_j = 1$ can be minimized. In other cases, standard errors in y are proportional to y, and the sum of squares of the *relative* errors should be minimized. This requires setting $w_j = [y_j(\text{meas})]^{-2}$ in Equation 2. In some cases, standard errors in y may be neither absolute nor strictly relative and alternative weighting factors are required. This is the case for luminescence decay data obtained by photon counting, for which the random error in y(meas) is Poisson distributed,[12] i.e., proportional to $[y(\text{meas})]^{1/2}$. Here the proper weighting factor is $w_j = [y_j(\text{meas})]^{-1}$.

Nonlinear regression programs can be designed with a general error sum as in Equation 2, with the ability for the user to choose the proper weighting factor prior to execution. If known by measurement, the experimental variance of each y_j(meas) can be set equal to $(w_j)^{-1}$.[13]

Equation 2 involves the sum of squares of the differences in calculated and experimental values of y. It is a mathematical expression of the assumption that only the standard errors in y are significant. If random errors in x are also significant, an appropriately weighted function reflecting errors in both x and y should be minimized.[13] Such a case arises in nonlinear regression analysis of data from potentiometric acid-base titrations, for which the correct weighting factor needs to take into account errors in both the volume of titrant V and the pH. Here, x = V, y = pH, and the proper weighting factor was shown[14] to be $w_j = [s_y^2 + s_x^2(dy/dx)_j^2]^{-1}$, where s_y^2 and s_x^2 are variances of the measured values of y and x, respectively, and $(dy/dx)_j$ is the slope of the titration curve at point j.

D. Matrix Representation

So far this review has relied mainly on conceptual, algebraic descriptions of regression analysis because it is felt that most readers will be more familiar with this approach. In reality, many regression programs use matrix methods in the so-called "batch formulation".[15] In such programs, the general model in Equation 1 is expressed in matrix notation:

$$[Y_c] = [f(x_j)]^t[B] \qquad (6)$$

where $[Y_c]$ is the computed model matrix, $[f(x_j)]^t$ is the transpose of a column matrix expressing the model functionality $f(x_j)$, and [B] is a row matrix containing the k + 1 parameters. If [Y] is the matrix corresponding to the measured data, then in terms of our earlier discussion, the error sum S becomes:

$$S = [Y - Y_c]^t[Y - Y_c] \qquad (7)$$

Equation 7 is the matrix equivalent of Equation 2. Weighting factors may be included if necessary. We return to this approach later in discussing some applications of nonlinear regression to multivariate spectroscopic data.

E. A First Example

Nonlinear regression analysis of a set of first-order kinetic data is now discussed in detail to illustrate how a typical analysis is set up and interpreted. We use Equation 4 with B = 0 to analyze a set of simulated absorbance vs. time data with normally distributed absolute error which is independent of the magnitude of the measured absorbance. In this example, y = absorbance and x = time. The latter is considered free of error. Thus, only the random errors in y are significant and S in Equation 2 can be minimized with $w_j = 1$. There are two parameters: B(0) = k and B(1) = A′, with true values B(0) = 0.100 and B(1) = 1.00. The data were analyzed by the Marquardt method using the program in Reference 3. As mentioned previously, this program (in BASIC) is interfaced with a graphics routine in our laboratory on an IBM/PC-XT configured microcomputer. Data are input either from a disk file or typed into a DATA statement. In response to initial dialogue, the user inputs starting values of the parameters and then views a graph of experimental and computed data. If agreement between the two plots is reasonable, the user begins the regression analysis. In many analyses, reasonable initial agreement may require simply that both plots fall within the same coordinate axis space on the monitor. If agreement is judged unsatisfactory, a new set of initial parameters can be chosen to give a better graphical comparison.

In our example, the Marquardt nonlinear regression analysis converged in six cycles (Table 1). When run by using a compiler such as TURBO BASIC, execution is complete in a few seconds. The standard deviation of the regression (SD) of 3.482×10^{-3} is about 0.5% of the largest y-value, about the same as the amount of absolute random noise added to the simulated absorbances. Values of the computed parameters B(0) and B(1) are essentially identical with their true values. Computed values are given with their standard errors, small relative values of which are good indicators of a satisfactory fit and of the significance of the parameters in the model. Initial guesses are recorded in the output since the influence of these should be investigated. Calculated and measured data and their differences are tabulated for the user's inspection. For comparison, regression analysis with the program in Reference 2 using a similar starting point gave B(0) = 0.100049, B(1) = 1.00012, and $SD = 3.617 \times 10^{-3}$ on a TRS-80 Model I microcomputer, but in 32 cycles rather than 6.

The next entry in the printed output (Table 1) is a correlation

Table 1
Test Run — First-Order Kinetics, Normally Distributed Noise Added

Matrix Condition Number = 32.62491
Convergence in* 6 *cycles
SD = 3.481837E-03
Sum delta squared = 1.454783E-04
Parameters and errors
B(0) = 0.1000196 ± 5.004599E-04
B(1) = 1.000075 ± 2.858538E-03
Initial guesses were:
B(0) = 0.15
B(1) = 0.97

(YC-Y/SD	YCALC	YMEAS	Independent variables
−0.89394	9.048874E-01	9.080000E-01	1.000000E+00
0.50550	8.187601E-01	8.170000E-01	2.000000E+00
−0.33597	7.408302E-01	7.420000E-01	3.000000E+00
2.10170	6.703178E-01	6.630000E-01	4.000000E+00
−1.00040	6.065168E-01	6.100000E-01	6.000000E+00
−0.06081	5.487883E-01	5.490000E-01	5.000000E+00
−0.70237	4.965545E-01	4.990000E-01	7.000000E+00
1.51996	4.492923E-01	4.440000E-01	8.000000E+00
−0.42262	4.065285E-01	4.080000E-01	9.000000E+00
−0.90899	3.678351E-01	3.710000E-01	1.000000E+01
−0.05044	3.328244E-01	3.330000E-01	1.100000E+01
0.32914	3.011460E-01	3.000000E-01	1.200000E+01
0.71309	2.724829E-01	2.700000E-01	1.300000E+01
−0.99147	2.465479E-01	2.500000E-01	1.400000E+01

Correlation matrix
1.0000E+00 8.0753E-01
8.0753E-01 1.0000E+00
Matrix product
1.0000E+00 −2.3842E-07
0.0000E+00 1.0000E+00

matrix. Its elements can be interpreted in a manner similar to the correlation coefficient between y and x variables in a linear regression. The off-diagonal elements of the matrix, i.e., those elements a_{ij} with $i \neq j$, give an indication of the correlation between the pairs of parameters with the [row, column] index of that element. The only off-diagonal element in the present example gives the correlation coefficient between parameters 1 and 2. Diagonal elements of this symmetric matrix should be unity. In practice, correlation is usually not serious when off-diagonal elements are smaller than 0.98.[3] Two parameters in a regression model which are interdependent are said to be correlated. Their final values will depend on one another. If the correlation is total, it is impossible to obtain unique estimates for each parameter.

The matrix product output is the product of the coefficient derivative matrix and its inverse. Diagonal elements should be unity and off-diagonals smaller than about 10^{-5} when the program is run in single precision. Larger off-diagonal elements suggest high correlation between parameters.

The final entry in the printed output is a deviation plot (Figure 2), a graph of the normalized deviation of each point, i.e., $\Delta y_j = [y_j(\text{meas}) - y_j(\text{calc})]/SD$ or its negative vs. x_j. This is sometimes called a normalized residual plot and the ordinate is in units of SD. The residual or "deviation" of the jth point is given by $dev = y_j(\text{meas}) - y_j(\text{calc})$. Figure 2 expresses *dev*/SD vs. time; an alternative is to plot data point number on the x-axis. A deviation plot is a more probing indicator of goodness of fit than summary statistics such as SD since adherence to the regression model is evaluated separately for each data point. A random scatter of points in the deviation plot around $\Delta y = 0$ indicates that the regression model adequately describes the data. Note that points in the deviation plot in the present example are randomly scattered, suggesting a good fit of the model to the data. However, if there are no *systematic* errors in the measurements and the deviation plot is not random but arranged in a pattern, then the form of the model should be judged incorrect. As a supplement to this interpretation, SD should be compared to the standard error (e_y) in measurement of y. The relation SD $< e_y$ suggests a rather good fit, and small nonrandom deviations in such instances can often be traced to small systematic errors in measuring y. Systematic errors of measurement can often be uncovered by analysis of data on standard systems known to follow the regression model. Deviation plots in conjunction with summary statistics such as SD are highly recommended for evaluating the quality of fit of the model to the data. As is discussed later, the information in nonrandom deviation plots can lead to identification of the correct model by a procedure known as "deviation pattern recognition".[1]

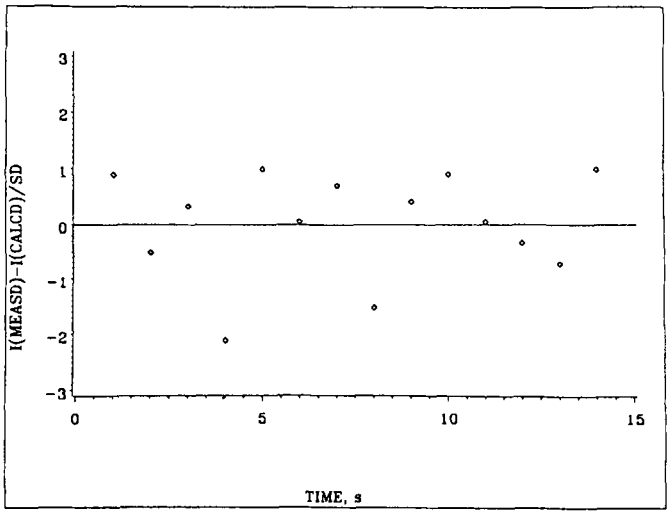

FIGURE 2. Deviation plot resulting from nonlinear regression example in Table 1.

III. MODEL BUILDING

A. Instrumental Response Curves

We use here the term "response curve" to denote a series of data points obtained as a measured instrumental response vs. either time or an experimentally controlled variable. Familiar examples are spectral absorbance vs. wavelength, current vs. potential, and luminescence intensity vs. time. The measured response, i.e., absorbance, current, or intensity, can be considered a dependent variable. Wavelength, potential, or time are the respective independent variables. Regression models for such curves should quantitatively express contributions to the measured response from the chemical and/or physical events being studied as well as nonrandom noise and other instrumental factors. Important instrumental contributions may include finite background offset, drift, instability, detection of the source, and any other characteristic of the measuring system which yields a finite signal. We refer to these instrumental signatures collectively as "background". If such background contributions are reasonably constant with time or highly predictable, they can often be measured and subtracted from the data. However if the background can be described in mathematical form, it is sometimes preferable to include specific terms in the model accounting for its contribution. An example is Equation 4, where a constant background B was included in the model for response y as a function of independent variable t. If the background contribution drifts linearly with time, B could be replaced with mt + B, representing a linear background with slope m and intercept B at t = 0. Other examples of models for background response are discussed in the following sections.

1. Closed-Form Theoretical Equations

Although not always available, closed-form theoretical relations between instrumental response and independent variables are ideal starting points for regression models. When used with the addition of appropriate background models, computations are usually fast, and physically significant parameters are obtained. As an example, we turn to sigmoid-shaped relations between current (i) in an electrochemical cell at a working electrode with controlled, linearly varying potential (E). The sigmoid form of response curve is found in DC polarograms and normal-pulse and rotating disk voltammograms. It is observed for linear sweep voltammograms in special kinetic situations and for experiments with very small "ultramicroelectrodes" of radius <10 μm at low scan rates, e.g., <20 mV s^{-1} (Figure 3). Such sigmoid-shaped i-E response curves as a class can be called steady-state voltammograms. The simplest electrode process giving rise to a sigmoid response is fast one-electron charge transfer uncomplicated by chemical reactions of the reactant (O) or product (R):

$$O + e = R \quad (E^{o\prime}) \tag{8}$$

Equation 8 represents a reversible transfer of one electron from an electrode to an electroactive species O. Electrochemists call such a reaction reversible when electron transfer is fast in both directions with respect to the time scale of the experiment. The i-E curve centers around the formal potential $E^{o\prime}$, which is the same as the half-wave potential ($E_{1/2}$) if the diffusion coefficients of O and R are equal. The half-wave potential is the value of E when the current is one half of the current at the plateau, called the limiting current (i_l). The equation[16] describing the steady-state voltammogram for a reversible electron transfer (Equation 8), assuming only O is initially present in the solution, is

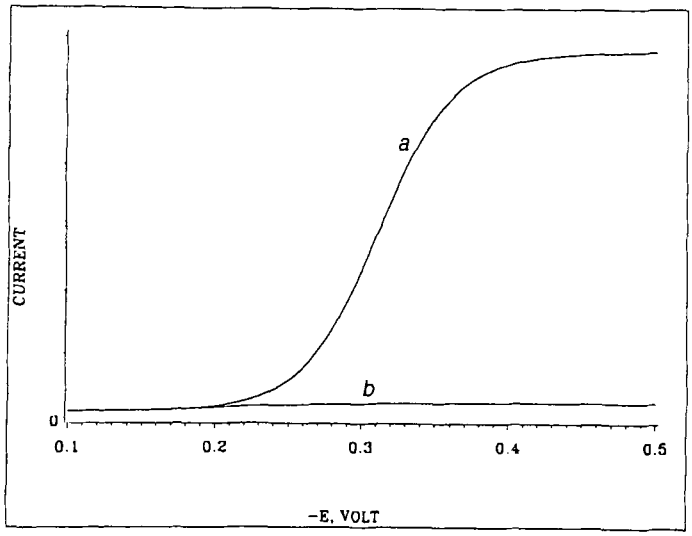

FIGURE 3. Graphical representation of the model for a steady-state voltammetric i-E response curve. (a) Faradaic component caused by reduction of O including linear background as in Equation 10; (b) background component alone, m(E'-E) + b.

$$i = i_l/1 + \theta) \tag{9}$$

where $\theta = \exp[(E-E^{o\prime})/S']$, $S' = RT/F$, R is the universal gas constant, F is Faraday's constant, and T is the temperature in degrees Kelvin.

For a well-resolved voltammogram, experience[16,17] has shown that an appropriate model for regression analysis combines Equation 9 with a linearly increasing background current:

$$i = i_l/(1 + \theta) + m(E' - E) + i' \tag{10}$$

The first term on the right-hand side of Equation 10 expresses the Faradaic current; the second two terms describe the contribution of background. E' is an arbitrary potential often chosen to fall before the initial current rise so that a background current i' at E' can be measured, and m is the slope of the background current (Figure 3). In a nonlinear regression analysis using Equation 10, the parameters determined are usually i_l, S', and $E^{o\prime}$. Since E' and i' are correlated,[18] E' is usually fixed. A slope correction factor accounting for nonparallel plateau

and baseline may also be included.[16] The quantities i′ and m may be used as regression parameters, or they can be kept fixed. In the latter case, values of i′ and m measured from data obtained at potentials before the onset of the wave can be input to the program. If i′ and m are fixed, a three-parameter fit is required. A five-parameter fit is needed if i′ and m are to be estimated by the regression analysis. Alternatively, experimentally measured or linearly extrapolated background (prior to the initial current rise) can be subtracted from the raw data prior to regression analysis onto Equation 9. Although there may be arguments in favor of one or another of these approaches, in practice we have found only small differences in most applications between such three- and five-parameter regression analyses. This appears to be generally so for data obtained with conventional-sized analytical electrodes as long as the background is well approximated by the linear model and S/N is sufficiently large, e.g., >100. For carbon fiber ultramicroelectrodes, we obtained better results by direct analysis of the raw data with inclusion of m and i′ in the model (see Section IV.A).

Meites and Lampugnani[16] pioneered nonlinear regression of sigmoid i-E data in applications to DC polarography. They resolved severely overlapped sigmoid waves by using a model composed of one term on the right-hand side of Equation 9 for each of two electroactive components (denoted as 1 and 2), as shown below:

$$i = i_l[f/(1 + \theta_1) + (1 - f)/(1 + \theta_2)] \qquad (11)$$

They presubtracted the linearly extrapolated background current and used S_1, S_2, $E^{o\prime}{}_1$, $E^{o\prime}{}_2$, and f, the fraction of component 1 in the mixture, as parameters. Here, S_1 and S_2 are contained in the $\theta_k = \exp[(E - E^{o\prime}{}_k)/S_k]$ for k = 1,2. Regression of polarograms onto Equation 11 was used to determine Pb(II) and Tl(I), which differ in half-wave potential by only about 50 mV, in two-component mixtures.

DC polarograms consisting of the signal for reduction of a single component overlapped with the final rise in residual current were resolved by adding a term exponential in E to Equation 9.[16] The exponential approximately describes the rising portion of the irreversible reaction responsible for the final current rise at the negative potential limit of the working electrode system. This model has been quite useful in analyzing linear sweep voltammograms (LSV) for kinetic studies of electrocatalytic reductions,[17,18] as discussed below.

The LSV experiment involves a linear scan of potential at a stationary working electrode in a quiet solution in an electrochemical cell. The shape of the measured i-E curve is characteristic of the mechanism of the electrode reaction which controls the flow of Faradaic current. In most cases, closed-form equations are not available for LSV i-E curves. However, expressions of the form of Equation 9 are applicable in some kinetic situations. One of these arises in redox electrocatalysis, in which a catalyst (P) added to the solution mediates electron transfer between the electrode and a soluble substrate (A) in solution, as illustrated below for reduction of A:

$$P + e = Q \quad \text{(at electrode)} \quad (E^{o\prime}) \qquad (12)$$

$$Q + A \xrightarrow{k_l} P + B \qquad (13)$$

An analogous reaction scheme could be written for electrocatalytic oxidations. Substrate A is not directly reducible at the electrode at potentials close to $E^{o\prime}$. The product of the electrode reaction (Equation 12), Q, reacts with A in a thin layer of solution close to the electrode. This homogeneous step (Equation 13) regenerates P at the electrode, increasing the current and changing the shape of the LSV curve from that in the absence of A. When the reduction is pseudo-first-order in Q and under kinetic control of the homogeneous electron transfer step (Equation 13), a sigmoid i-E curve described by Equation 9 is observed. The limiting catalytic current, i_l, can be used to find the concentration of A (C^*_A), the concentration of B (C^*_B), or the chemical rate constant k_l from the expression:

$$i_l = FA'C^*_P(D_PC^*_Ak_l)^{1/2} \qquad (14)$$

where A′ is the area of the electrode, D_P is the diffusion coefficient of P, and the C*'s denote concentrations in the bulk of solution.

For some redox electrocatalytic reactions, although substrate is not reduced at $E^{o\prime}$, it may be slowly (irreversibly) reduced at the electrode at potentials slightly more negative than $E^{o\prime}$. The requirement for pseudo-first-order kinetics dictates that C^*_A exceeds 10 × C^*_P. Because of this large excess of A, the i-E curve for its slow direct reduction may overlap the catalytic i-E curve. Since irreversible reduction current has an exponential dependence on E in the rising portion of its LSV curve, the following regression model can be used:

$$i = i_l/(1 + \theta) + i''\exp[S''(E'' - E)] + m(E' - E) + i' \qquad (15)$$

Here, i″ is the background current due to direct reduction of A at a second arbitrary potential E″ chosen to be past the catalytic wave, $S'' = \alpha'F/RT$, where α′ is the effective electrochemical transfer coefficient for the direct irreversible reduction of substrate. The other parameters are the same as in Equation 10. Equation 15 is a model built up from the electrocatalytic current described by the first term on the right-hand side, an exponential background term accounting for direct reduction of substrate, and a linear background term. The observed signal is assumed to be the sum of these three components.

There are several alternatives for nonlinear regression of

steady-state electrocatalytic data with an exponential background component: (1) raw data can be analyzed directly by using Equation 15 with the parameters i_l, S′, E°′, i′, i″, S″, and m; (2) a linearly extrapolated residual current can be subtracted from the raw data and the parameters i_l, S′, E°′, i″, S″ used with m and i′ in Equation 15 fixed at zero; and (3) separately measured background i-E data for direct reduction of the substrate alone can be subtracted from the raw data and Equation 9 used with parameters i_l, S, E°′. The latter three are the important quantities here, especially i_l which can yield k_l, C^*_A, or C^*_P via Equation 14. The values of the background parameters are incidental in most applications. As long as correlation is low for i_l, S′, and E°′ with any of the other parameters, any of the choices should be appropriate. However, total background subtraction requires a second separate experiment.

In situations where the background current can be accurately modeled, we have argued against background subtraction since significant background signals are not likely to be accurately reproduced from scan to scan and because subtraction causes an increase in noise in the resultant i-E curve by propagation of errors.[18] When analysis of LSVs for the pseudo-first-order electrocatalytic reduction of 4,4-dibromobiphenyl with anthracene as the catalyst was done with the above-mentioned approaches (2) and (3), the analysis including the exponential-term parameters gave about twofold better precision in SD and k_l compared with the total background subtraction method. Thus, regression of data onto Equation 15 with m and i′ fixed at zero allowed calculation of the catalytic component of the response curve[18] (Figure 4). Here, the exponential background was a sizable fraction of the observed current at potentials of the limiting current. For data from similar experiments where catalysts were photoexcited,[17] essentially no difference in results was found in analyzing data with [method (2)] and without [method (1)] linear background subtraction. In this case, photoexcitation increased the effective rate constant tenfold or more, increasing S/N such that the relative contribution of the background was small. In practice, all three approaches to using Equation 15 can give acceptable results if S/N is large enough and the residual current is accurately modeled and reproducible. The choice for each case should be made separately based on the characteristics and S/N of the available data.

2. Empirical Models: Peak-Shaped Data

Nonlinear regression is often used with empirical models. Many types of single and overlapped peak data from UV-VIS absorbance, fluorescence, X-ray photoelectron (XPS), and NMR spectroscopy can be reliably fit by a linear combination, as in Equation 16, of Lorentzian [L] and Gaussian [G] peak shapes, where:

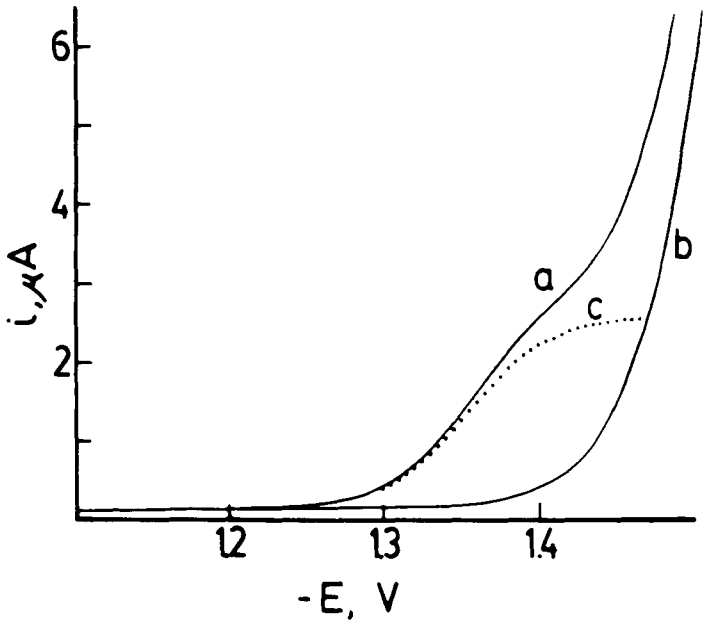

FIGURE 4. Linear sweep voltammograms at a hanging drop mercury electrode at 200 mV s^{-1} for reduction of 4,4′-dichlorobiphenyl (DCB) in 0.1 *M* tetrabutylammonium iodide (TBAI) in DMF. (a) Electrocatalytic reduction with 0.1 m*M* anthracene as catalyst and 4.0 m*M* DCB; (b) direct reduction of 4.0 m*M* DCB; (c) catalytic component of the curve in (a) recomputed from the parameters found by nonlinear regression. (Reprinted from Rusling, J. F. and Connors, T. F., *Anal. Chem.*, 55, 776, 1983. With permission. Copyright 1983, American Chemical Society.)

$$y = h\{fG + (1 - f)L\}$$

$$L = W^2/[(x - x_o)^2 + W^2]$$

$$G = \exp\{-(x - x_o)^2/2W^2\} \qquad (16)$$

where f is the fraction of Gaussian character, h is peak height, W is half-width at half height, and x_o is peak position, These four parameters are usually used in the regression analysis.[19-21] Product functions of G and L have also been used for XPS.[20] Figure 5 illustrates a fit by nonlinear regression to a three-peak model of data from high resolution XPS. The data represent the Cls XPS spectrum of a highly polished glassy carbon surface.[19] The main peak is assigned to graphitic carbon, and the shoulders at higher binding energies correspond to C–O and C=O species on the surface. The three-peak model consisted of the sum of three equations of the type of Equation 16, one for each peak. It included both linear and sigmoid background terms[19-21] to account for the characteristics of the instrument. Following convergence, the shapes of the three peaks were reconstructed from the best values of the parameters. Numerical integration of each resolved peak then yielded an estimate for the amount of each type of carbon on the surface. This is an

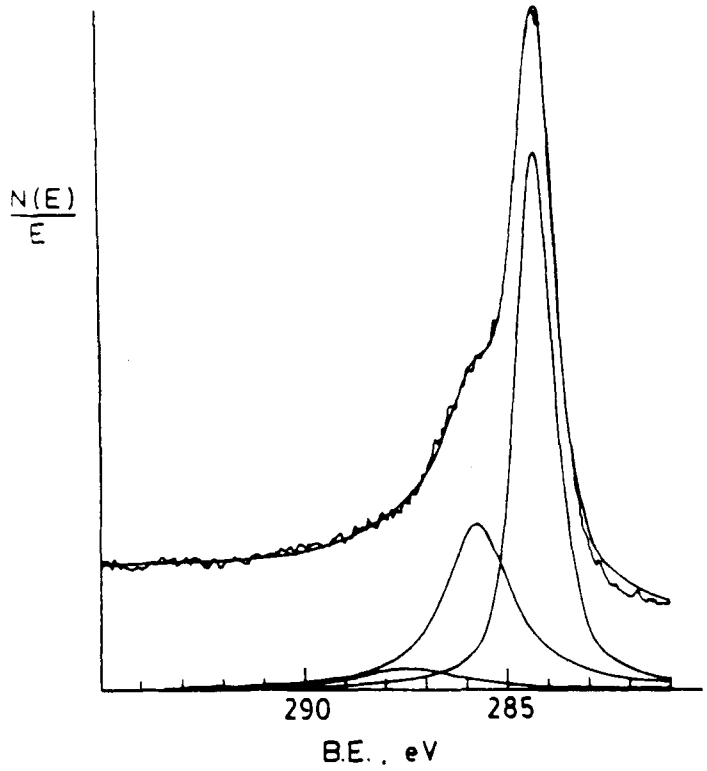

FIGURE 5. Results of nonlinear regression analysis of C(1s) XPS spectrum of highly polished glassy carbon onto a three-peak model. The upper curve shows the experimental data and the best regression line. The lower three curves are the individual components computed from the best values of the regression parameters. (Reprinted from Kamau, G. N., Willis, W. S., and Rusling, J. F., *Anal. Chem.*, 57, 545, 1985. With permission. Copyright 1985, American Chemical Society.)

example where instrumental characteristics require a slightly more complicated form than previously discussed to account for the background signal.

A second application of Equation 16 involves fitting the fluorescence spectrum of pyrene in micellar solutions. The relative intensities of the overlapped vibronic peaks in the spectrum can be used to probe the environment in which pyrene is solubilized.[22] Individual peak intensities and areas of the vibronic peaks change in different microenvironments, so that accurate knowledge of these quantities in known solvent environments allows for comparison of fluorescence spectra of pyrene bound to surfactant aggregates. We have used regression procedures similar to those discussed for XPS with Equation 16 as the basic peak model to show that pyrene experiences a rather hydrophilic environment when bound to surfactants such as 0.1 *M* sodium dodecylsulfate (SDS). That is, relative areas under the vibronic peaks of pyrene in 0.1 *M* SDS were similar to those found for spectra in water and methanol and different from those found in hexane. These results suggested that the solute resides close to the micelle-water interface.

B. Numerically Solvable Equations

In many cases, models for experimental data cannot be expressed as closed-form equations, i.e., no explicit expression of the form of Equation 1 can be found. This is not a limitation to nonlinear regression provided that a numerical approach is used that does not require closed-form derivatives of the model. Then, a numerical method to compute y_j(calc) at the required values of x_j is all that is needed. One of the simplest cases is when the model takes the form of $F(x,y) = 0$. A procedure to solve such equations numerically for y_j(calc) is discussed first, followed by several examples of its use.

1. The Newton-Raphson Method

Polynomial expressions in y of a degree higher than two or of a fractional degree can be solved by using iterative approximation methods. A widely used procedure is the Newton-Raphson method.[7,23] If the equation to be solved is of the form $F(y) = 0$ and the initial guess of the root is y_k, then the Newton-Raphson procedure dictates that a better approximation, y_{k+1}, for the root is given by:

$$y_{k+1} = y_k - F(y_k)/F'(y_k) \qquad (17)$$

where $F(y_k)$ is the function evaluated at y_k and $F'(y_k)$ is the first derivative of the function evaluated at y_k. Derivation, limitations, and examples of programming for several applications have been presented.[7,23] In practice, the method works well for well-conditioned problems if a good initial estimate is provided. Equation 17 is then used repeatedly until convergence to a preset limit (LIM) is reached. A typical convergence criterion is

$$\text{ABS}[(y_{k+1} - y_k)/y_{k+1}] \leq \text{LIM}$$

where LIM may be set at 0.0001 or smaller, as desired. Given a good initial estimate, convergence is rapid for well-conditioned applications and is often reached in a few cycles. Equations other than polynomials can also be solved by the Newton-Raphson approach.

We turn again to steady-state voltammetry for an example of the use of the Newton-Raphson method within a model subroutine of a nonlinear regression program. The shape of the steady-state voltammogram is sensitive to the electrode reaction mechanism. For an electrodimerization reaction:

$$O + ne = R \qquad E^{o\prime}$$
$$2R \rightarrow R\text{–}R \qquad (18)$$

the equation[24] of the steady-state voltammogram is

$$i + \theta i^{2/3} - i_l = 0 \qquad (19)$$

where θ is the exponential function of E used in Equation 9. Here,

$$F(i_k) = i + \theta i^{2/3} - i_l$$

$$F'(i_k) = 1 + (2/3)\theta i^{-1/3} \quad (20)$$

In the subroutine used to fit experimental data, the Newton-Raphson method was used to obtain the best approximate root i_j(calc) at each E_j by using Equation 17 with LIM = 0.00001 as the test for convergence. The measured currents at each E_j were used as initial estimates of the roots. Logical statements were included to terminate any Newton-Raphson routine after 50 iterations to avoid infinite loops which could arise during the course of the regression analysis. Regression onto Equation 19 with the parameters E°′, S′ = RT/F, and i_l was applied to confirm the electrodimerization mechanism for the voltammetric reduction of pyridinecarboxylic acids,[24] acetophenone, and 3-formylpyridine.[25]

C. Equilibrium Models: Law of Mass Action

Equilibrium models can be used to describe experimental data in many types of experiments. Acid-base and other titration data have been extensively analyzed by nonlinear regression analysis with equilibrium models.[1] The most impressive early result of studies by Meites and co-workers was that the concentrations of both analyte and titrant could be determined with good precision by the regression analysis, i.e., the titrant need not be precisely standardized! More recent work showed the possibility of detecting a 1% acidic impurity in solutions of an acid with a pK_a differing from the impurity by only 0.57 units.[26] Thus, nonlinear regression analysis can greatly extend the applicability of conventional titration methods. As mentioned previously weighting functions for the error sum with expressions reflecting the errors of both measured pH and volume of titrant have been recommended[14] and the factors affecting precision have been explored quantitatively for acid-base titrations.[27] The reader is referred to the original literature[1,13,23,26,27] for details.

The example following deals with multiple equilibria. The approach used is similar to treatments of multisite binding equilibria of ligands to macromolecules as described by Tanford[28] and Wyman.[29]

1. Oligomerization and Deviations from Beer's Law

Dye molecules such as phthalocyanines form dimers and higher oligomers in solution. To establish the nature of the species in solution, equilibria of 10^{-5} to 3×10^{-4} *M* iron(II) and cobalt(II) phthalocyanines (FePc and CoPc) in 0.1 *M* LiCl in DMSO were studied by UV-VIS spectroscopy.[30] A major peak in the 650- to 660-nm region with a second smaller band near 595 nm were found (Table 2). No separate peak attributable to a dimer was found in DMSO solutions of CoPc, but a peak caused by absorbance of an association dimer at 630 nm was found for FePc at concentrations $>7 \times 10^{-5}$ *M*. However, absorbances (A) of these systems did not obey the Beer-Lambert law, showing negative deviations for the monomer peak throughout the range of concentrations studied. Preliminary nonlinear regression analysis showed that a single dimerization equilibrium was insufficient to explain the A vs. monomer concentration (C_M) data. Thus, stepwise equilibria were expressed via the overall equilibrium as follows:

$$nM = M_n \qquad K^n = [M_n]/[M]^n \quad (21)$$

Here, M is the monomer, M_n is the highest (nth degree) aggregate, C_M is the total concentration of MPc in all forms, and K^n is the overall formation constant for M_n, formulated in this way for ease of computation and to minimize the number of parameters. K^n represents the product of n-1 stepwise formation constants, analogous to an overall formation constant in complexation equilibria. The mass balance for the monomer is given by:

$$C_M = [M] + n[M_n] \quad (22)$$

Table 2
Standard Deviations from Regression Analyses on Equilibrium Spectroscopic Data for MPc's

CoPc[a]

n	λ, nm = 654	660	664
2	0.1082	0.0957	0.0820
3	0.0798	0.0660	0.0557
4	0.0625	0.0507	0.0436
5	0.0528	0.0443	0.0406
6	0.0477	0.0428	0.0421
7	0.0451	0.0439	0.0451
8	0.0440	0.0459	
9	0.0437		
10	0.0941		
$10^{-4}e_l$	7.1 ± 0.32	7.69 ± 0.26	7.1 ± 0.22
mean K (n = 6)		1369 ± 124	

FePc[a]

n	λ, nm = 654	660	670
2	0.0364	0.0516	0.0296
3	0.0206	0.0296	0.0201
4	0.0290	0.0247	0.0210
5	0.0400	0.0298	0.0256
$10^{-4}e_l$	7.32 ± 0.27	7.20 ± 0.41	4.42 ± 0.20
mean k (n = 3)		337 ± 46	

First set of rows are SD of regressions for fits of equilibrium data onto Equations 23 and 24. Parameter values given with standard errors; e_l is molar absorptivity.

Reprinted from Owlia, A. and Rusling, J. F., *J. Electroanal. Chem.*, 234, 297, 1987. With permission. Copyright 1987 Elsevier.

Combination of eqs 21 and 22 yielded an n-th order equation in [M]:

$$nK^n[M]^n + [M] - C_M = 0 \quad (23)$$

The total absorbance A at wavelengths near the 660-nm maximum was first considered to be the sum of that from the monomer and the nth oligomer:

$$A = b(e_1[M] + e_2K^n[M]^n) \quad (24)$$

Experimental data of A vs. C_M at fixed wavelength were analyzed by nonlinear regression analysis onto a model composed of Equations 23 and 24. Equation 23 was solved by the Newton-Raphson method to provide values of [M] to Equation 24. Preliminary analyses with this model using K^n and the molar absorptivities e_1 and e_2 as regression parameters showed that the computed value of e_2 was not significant at wavelengths near to or larger than the maximum. Thus, A vs. C_M data were analyzed with a two-parameter (K^n and e_1) model, assuming monomer as the only absorbing species at the wavelength of interest. The value of the integer n was successively increased and the goodness of fit for each n was assessed by examining SD of the regression and deviation plots of residuals. Best fits were obtained for n = 3 or 4 for the FePc data, while higher values were found for CoPc (Table 2). Good agreement between computed and experimental absorbances (Figure 6), nonrandom deviation plots for analyses yielding higher SD, and random deviation plots for n-values with minimum SD confirmed the goodness-of-fit conclusions based on SD. Thus, results of the regression analyses suggest

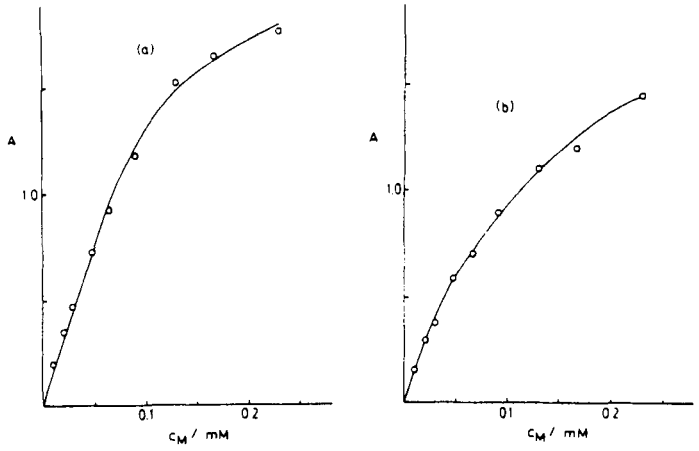

FIGURE 6. Influence of metal phthalocyanine concentration on absorbance in 0.1 *M* $LiClO_4$ in DMSO. Circles are experimental data. (a) Co(II)Pc at 660 nm, line computed from nonlinear regression onto Equations 23 and 24; (b) Fe(II)Pc at 654 nm, line computed from nonlinear regression onto Equations 23 and 24. (Reprinted from Owlia, A. and Rusling, J. F., *J. Electroanal. Chem.*, 234, 297, 1987. With permission. Copyright 1987 Elsevier Sequoia S.A.)

that CoPc is more extensively aggregated than FePc in DMSO. Although data could have been analyzed by a stepwise equilibrium model, such models contain excessive numbers of parameters not warranted by the precision of the absorbance data. In the above application, the information desired was mainly the relative degree of aggregation of CoPc and FePc, and the analysis used was sufficient to establish significant differences in aggregation between the two compounds.

It is often desirable to confirm features of a regression model by independent experiment. In the MPc systems, dilution of nearly saturated solutions of either MPc in DMSO containing 0.1 *M* LiCl resulted in an increase in absorbance at λ_{max} with time over about 1.6 h.[30] These results confirmed the presence of higher aggregates. Other applications of multiple equilibrium models with unknown stoichiometry are discussed in Section IV.E.

D. Digital Simulation — Linear Sweep Voltammograms

As mentioned previously, closed-form equations for i-E curves in LSV can be derived only in a limited number of special cases. In general, the partial differential equations describing diffusion and kinetics in LSV must be solved by using a numerical method to compute response curves. This situation is common to several experimental techniques, and the LSV case is discussed here in detail.

A variety of sophisticated methods are available for numerically solving partial differential equations.[31] The one discussed here is an explicit finite difference technique called "expanded space grid digital simulation".[4,32,33] It provides rapid and accurate computation of theoretical LSV response curves for, in principle, any electrode reaction. Since electrode geometry should be included for an accurate model, the expanded grid simulator is described here for a spherical electrode. Essentially, diffusion and kinetics of electrochemical reactions are simulated by setting up around the electrode a hypothetical grid of volume or space elements with exponentially expanding widths (Figure 7). Changes in concentrations of reaction participants due to diffusion and chemical kinetics are computed separately for each space element. For a spherical electrode, the area (A'_j) of the outer boundary of the jth space element is given by:

$$A'_j = 4\pi(r_o + r_j)^2 \quad (25)$$

where r_o is the radius of the electrode, and r_j is the distance of the boundary from the electrode surface. Other electrode geometries are accommodated by changing the form of Equation 25.

A qualitative overview of the model's use is now given. The reader is referred to the original literature[4] for specific equations and computational details. The duration of the LSV experiment is broken up into small uniform time elements. For an uncomplicated charge transfer reaction such as Equation 8, when only

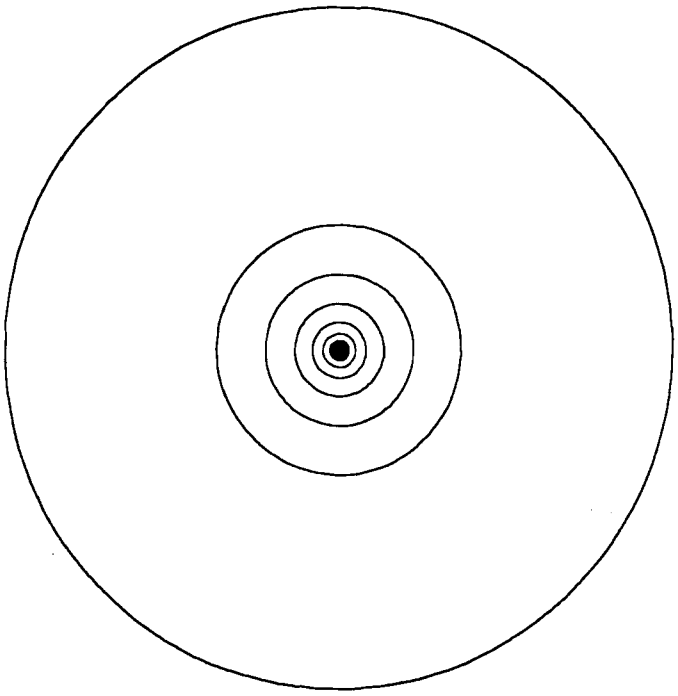

FIGURE 7. Two-dimensional representation of volume elements used for exponentially expanding grid digital simulation of linear sweep voltammograms at a spherical electrode represented by dark center disk.

A is initially present in solution, initial conditions are $C_j^A = C_A^*$ and $C_j^B = 0$, where C_A^* is the bulk concentration of A, and C_j^A and C_j^B are the concentrations of A and B in the jth space element. Simulating the LSV experiment consists of performing the following steps successively for each element:

1. Fick's diffusion laws and the equations for electrode kinetics are used to compute the flux of A and B in the space element closest to the electrode. The greater importance of space elements close to the electrode in computing this flux is the reason for exponentially decreasing the size of the space elements closer to the electrode. Thus, the exponential grid has a better "resolution" closer to the electrode where changes in concentration of A and B are more important to the electrochemical experiment.
2. The current is then computed from:

$$i = FA' \text{ (flux of A at electrode surface)} \quad (26)$$

where F is Faraday's constant and A' is the electrode area.
3. The changes in concentration (ΔC_j) of A and B resulting only from diffusion are computed for each space element.
4. The concentrations of A and B are obtained, e.g.,

$$V_j^A = C_j^A + \Delta C_j^A \quad (27)$$

where V_j^A is the concentration of A anticipated only from diffusion. If chemical kinetics are coupled to the charge transfer reaction, such as in Equations 12 and 13, the contribution to the concentrations from the applicable rate laws are added to the V_j to obtain the total concentrations in each space element.[4]

In LSV, each time element corresponds to a new point on the potential axis (i.e., since $E = E_o + \nu t$), so the simulation produces a computed i-E curve. For use in nonlinear regression, the simulator is placed in the model subroutine of the regression program. It includes parameters such as diffusion coefficients and heterogeneous and homogeneous rate constants. Results from nonlinear regression analysis of LSV data for the reversible reduction of 9,10-diphenylanthracene at a spherical mercury electrode in DMF are illustrated in Figure 8. Other applications are discussed in Section IV.

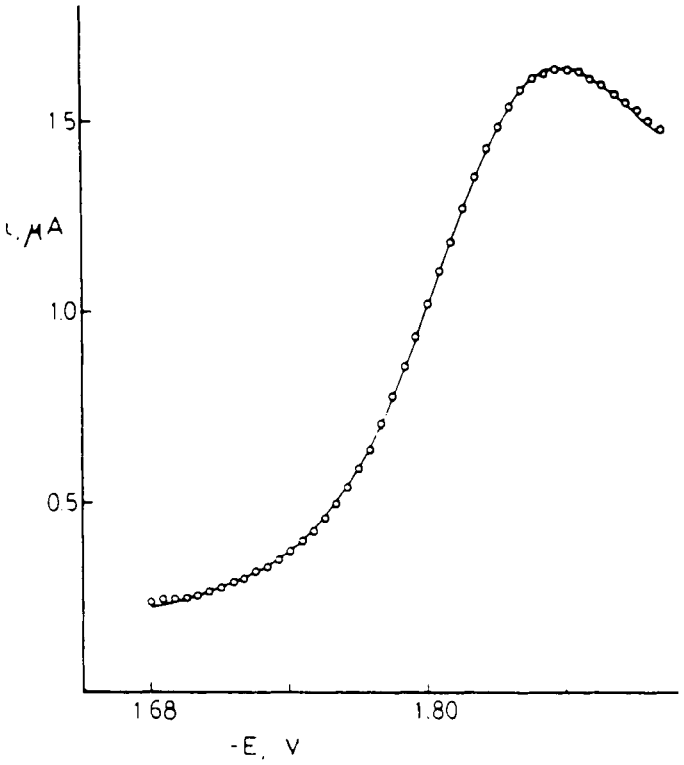

FIGURE 8. Reversible linear sweep voltammogram at a hanging drop mercury electrode at 0.20 V s^{-1} for 0.21 m*M* 9,10-diphenylanthracene in 0.1 *M* TBAI in DMF. Circles are experimental data; line from nonlinear regression/digital simulation. (Reprinted from Arena, J. A. and Rusling, J. F., *Anal. Chem.*, 58, 1481, 1986. With permission. Copyright 1986, American Chemical Society.)

E. Computational Errors

Since nonlinear regression is an iterative procedure, it is prone to the propagation of errors in repeated single-step calculations. This problem may be amplified when iterative or finite difference procedures are used to construct regression

models. Care must be taken that computational errors do not bias the results of regression analyses. This is best confirmed by analyzing a set of computer-simulated data to which has been added varying amounts of random noise. This procedure can confirm the correctness of the regression method before moving on to the analysis of real experimental data. The discussion following illustrates a few of the problems that may be encountered and suggests how they may be corrected.

1. Roundoff and Truncation Errors

Roundoff errors occur because computers must represent exact real numbers as finite decimals. For example, since the computer can only retain an n-digit representation of the fraction 2/3 = 0.6666666666....., it might represent 2/3 as 0.6666667. Rounding is inherent in arithmetic operations and is not a random process.[34] Double or multiple precision can often be used to minimize roundoff errors.

Truncation errors occur when an infinite series for a mathematical function is replaced by a finite one by eliminating less significant terms. Familiar subroutines used because of speed can lead to unacceptable errors in some applications. To illustrate this effect, consider a series approximation to the error function (erf), which appears in solutions of diffusion and other mass transport equations. The value of erf(x) for $0 \leq x \leq 2$ can be evaluated by a Maclaurin series:

$$\text{erf}(x) = [2/\pi^{1/2}][x - x^3/3 + x^5/(5 \cdot 2!) - x^7/(7 \cdot 3!) + x^9/(9 \cdot 4!) - \ldots] \quad (28)$$

It is often assumed that for $x \leq 0.1$ only the first term is necessary, but this truncation gives an error of 0.27% at x = 0.09 when compared with the exact function. An error of this magnitude could propagate seriously in repetitive computations. An alternative is to define the required accuracy as a limit of acceptable error or tolerance and evaluate each term in Equation 28 until the last term falls below this limit. By using this procedure with a tolerance limit of 10^{-6}, four terms of Equation 28 are needed for evaluation of erf(2.0) to 10^{-6} accuracy.[35] If tests of a series algorithm on simulated problems similar to the real application produce significant errors, then an approach similar to that described here may be warranted. On the other hand, errors traced to roundoff in exponential routines can sometimes be minimized by using double precision.

2. Finite Difference Approximations

In addition to applications in numerically solving differential equations, finite difference methods are often used for integration or differentiation. Numerical derivatives are sometimes used in regression programs. For a curve of the form y = F(x), the expression:

$$dy/dx = (y_j - y_{j-1})/(x_j - x_{j-1}) \quad (29)$$

can be used to approximate the derivative at $x_j - (x_j - x_{j-1})/2$. Derivatization is inherently unstable and amplifies error in the data. Assuming that x-values are error free, problems in a finite difference approach have been illustrated[36] by evaluation of $y_j = (1/3)^{j-1}$ from:

$$y_j = (10/3)y_{j-1} - y_{j-2}, \qquad j = 3, 4, 5, \ldots n \quad (30)$$

where $y_1 = 1$ and $y_2 = 1/3$. Values of y_j computed with Equation 30 on an 8-bit microcomputer in single precision diverged to large numbers at $n > 8$, e.g., giving $y_{19} = 2.24$ compared with the much smaller exact value of 2.581×10^{-9}. Double precision improved matters, but divergence to very small numbers occurred at $n > 16$. This example is rigged to propagate errors in differences between successively computed and rounded y-values, but similar problems can be encountered in using Equation 29 when $(y_j - y_{j-1})$ is small with respect to the standard error in y.

Clearly, reliable numerical derivatives require smoothing or filtering of the raw data. A critical examination of several options has been presented elsewhere.[37] In contrast to derivatization, numerical integration is more stable and averages random noise, improving S/N. The commonly used trapezoidal rule is a simple and reliable way to integrate data. Essentially, the area under the curve y = F(x) is broken up into a series of trapezoids with area:

$$A = (w/2)[F(x_{j+1}) + F(x_{j+2})]$$

The sum of the areas of all the trapezoids gives the integral or the total area under the curve. If the widths (w) of all trapezoids are equal, the area (A) under the curve from x_1 to x_n is given[7] by:

$$A = (w/2)[F(x_1) + F(x_n)] + w \sum_{j=1}^{n-1} F(x_1 + jw) \quad (31)$$

when n is the total number of trapezoids. Accuracy of the method is improved by making the width of the "slices" small.

3. Testing with Simulated Data

The errors discussed above illustrate only a few of those that could arise. Again, the necessity of validating the regression method as correct and free of serious parameter correlation by analyzing simulated data with known parameter values must be stressed. Data with noise of the expected experimental magnitude and statistical distribution are also useful to assess the effects of noise on the quality of the fit, the expected precision of the parameters, and the ability to distinguish between closely related models.

Random number generators on computers should not be used directly for generating noise because the numbers obtained are not truly random. A convenient way to add normally distributed noise is to first use the method of Box and Muller[38] to tranform

computer-generated "random" numbers to N normally distributed numbers z_j with zero mean and unit variance. Then, compute N theoretical values of y_j with a maximum value at y_{max}. Values of $y_{j,f}$ containing noise at an absolute fraction of y_{max} are given by:

$$y_{j,f} = y_j + fz_j y_{max} \quad (32)$$

The resulting noise is dependent on the maximum signal only, i.e., it is absolute noise. Data with noise proportional to $y_{j,f}$ or $y_{j,f}^{1/2}$ can be generated by a substituting these respective quantities into Equation 32.

IV. SELECTED RECENT APPLICATIONS

A. Steady-State Voltammetry

1. Studies with Conventional Electrodes

Examples of analyzing steady-state voltammetric data were discussed above, mainly in the context of the reversible electrode reaction in Equation 8. Nonlinear regression of steady-state voltammograms was used as the basis for an automated method of classifying the voltammetric data with respect to the electrode reaction mechanism giving rise to it.[25] Details of this classification method are discussed in Section V. In addition to mechanistic discrimination, it was found that analysis of steady-state voltammograms could provide simultaneous estimates of the apparent standard heterogeneous rate constant (k^o) for electron-transfer across the electrode-solution interface, the electrochemical transfer coefficient (α), and standard potential (E^o) for the reaction when k^o was of intermediate magnitude.[25] For rotating disk voltammetry (RDV) at a rotation rate of 1800 rpm, the applicable range was $0.02 \leq k^o \leq 0.0002$ cm s^{-1}. For example, regression analysis of RDVs gave a k^o of 0.0022 ± 0.0002 cm s^{-1}, $E^{o\prime}$ of 458 + 11 mV vs. NHE, and $\alpha = 0.635 + 0.006$ for the oxidation of ferrocyanide ion in neutral 0.5 *M* KNO_3 at a partially activated glassy carbon electrode. Precision was good, kinetic parameters agreed well with those for similar electrodes,[39] and $E^{o\prime}$ was in good agreement with the directly measured value[19] of 448 mV vs. NHE obtained at a fully activated glassy carbon electrode at which the reaction was reversible. The regression method was also used to study the kinetic effects of the aging of glassy carbon surfaces after activation by polishing.[39]

Steady-state LSV curves for electrocatalytic reductions of mono- and polyhalogenated biphenyls by a series of catalysts were analyzed using the model in Equation 15. The catalytic component of the current was separated from the overlapped signal for direct reduction of substrate by nonlinear regression analysis. The limiting catalytic current was then used to compute rate constants for homogeneous electron transfer between catalyst anion radicals and halobiphenyls via Equation 14. Deviation plots allowed the detection of catalytic behavior even when a catalytic peak was not visibly distinguishable from the overlapped exponential background.[18] The dependence of these rate constants on standard potential of the catalyst was then analyzed by nonlinear regression to yield the standard potentials and homogeneous electron exchange rate constants for the halopbiphenyls.[40] These latter parameters are not amenable to direct measurement by electrochemical methods for irreversibly reduced compounds.

Catalytic currents for the above reductions were further enhanced when the catalyst anion radicals formed at the electrodes were excited with light of wavelength in the visible range corresponding to their electronic absorption bands. Current-potential curves at illuminated electrodes under conditions pseudo-first order in the catalysts pyrene, anthracene, and 9,10-diphenylanthracene were found to give good quality fits to Equation 15 for the substrates chlorobenzene and 4-chlorobiphenyl (Figure 9). The i-E curves behaved like steady-state voltammograms and the limiting catalytic currents obtained from nonlinear regression could be used to estimate apparent rate constants (dependent upon light flux). Results demonstrated 16- to 12,000-fold rate enhancements for the photocatalyzed processes compared with the same electrocatalytic reactions in the dark.[17]

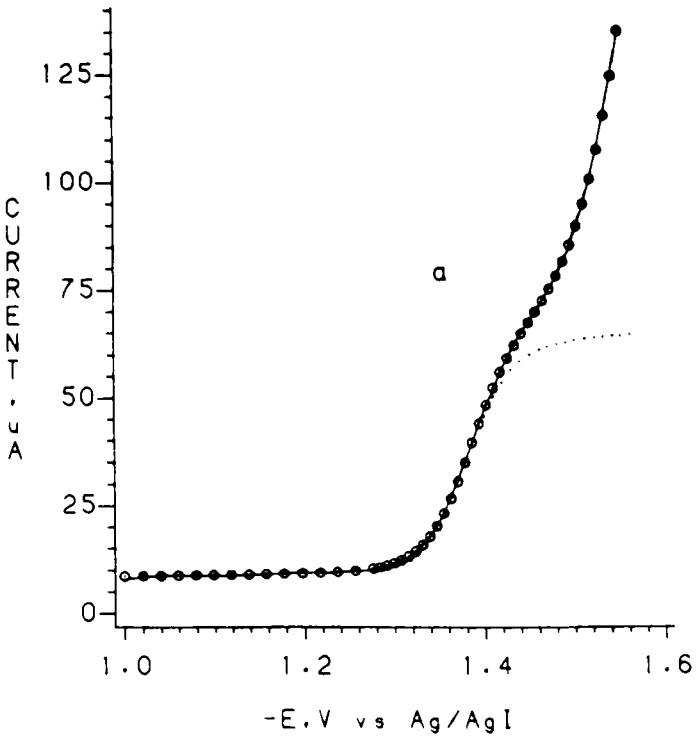

FIGURE 9. Linear sweep voltammogram of 0.38 m*M* 9,10-diphenylanthracene with a 40-fold excess of 4-chlorobiphenyl at 0.04 V s^{-1} in 0.1 *M* TBAI/DMF at a glassy carbon electrode illuminated by visible light. Solid line represents experimental data; circles computed by nonlinear regression onto Equation 15; dotted line is the catalytic component of the photocurrent computed from the best values of regression parameters. (Reprinted from Shukla, S. S. and Rusling, J. F., *J. Phys. Chem.*, 89, 3353, 1985. With permission. Copyright 1985, American Chemical Society.)

Reduction of the mitotic cycle regulatory hormone trigonelline (1-methyl-3-carboxypyridinium ion) at mercury electrodes was shown to involve adsorption by using nonlinear regression of DC polarograms. Data obtained in aqueous pH 1.7 buffers were corrected by subtracting the linearly extrapolated background. Although the polarographic data appeared to the observer as single waves, regression onto Equation 9, the model for a single polarographic wave, resulted in a nonrandom deviation plot with a shape characteristic for data from a two-wave system regressed onto Equation 9. Subsequent regression of these data using Equation 11, the two-wave model, yielded a random deviation plot indicating the correct model. Results were interpreted in terms of an adsorption prewave because the height of the wave determined by regression analysis reached a limiting value with increasing concentration of trigonelline. This limiting adsorption current indicated full surface coverage of the electrode with adsorbate. This allowed an estimation of the surface concentration that could not have been made without the regression analyses. Comparison with theoretical surface coverages for different molecular orientations suggested that the molecule was absorbed in a flat orientation on the surface of the electrode.[41]

2. Ultramicroelectrodes

Microelectrodes with dimensions in the micrometer range have received considerable attention recently. Because very small currents are generated at electrodes of very small area, such ultramicroelectrodes can be used in highly resistive media or at scan rates of thousands of volts per second. Diffusion is more efficient and capacitance is smaller at these tiny electrodes.[42] These factors result in improved S/N over that at larger electrodes. Unlike conventional-sized disk electrodes of 0.1 to 50 mm in radius, ultramicroelectrodes give sigmoidal-shaped, steady-state current potential curves at low scan rates under conditions of diffusional mass transport.[42] Thus, equations for i-E response at ultramicroelectrodes at low scan rates are of similar form to those for any steady-state voltammogram.

Nonlinear regression was applied to analysis of steady-state voltammograms obtained at carbon fiber disk microelectrodes of radius about 6 μm at scan rates ≤10 mV s^{-1}. Voltammograms for the oxidation of ferrocene in acetonitrile with 0.2 *M* $LiClO_4$ as electrolyte gave excellent fits when regressed onto Equation 10, the model for reversible steady-state voltammograms with linear background. In this case, including the background parameters in the model for analysis of the raw data gave significantly improved results compared with background subtraction followed by regression onto Equation 9. Relative SDs of the regression were <0.03% of the limiting current in all cases. Average parameter values found for seven sets of data were, RT/F = 0.02557 ± 0.00012 V (theory 0.2559 at 24°C); $E^{o\prime}$ = 0.3106 ± 0.0005 V vs. SCE (Reference 44, 0.311 V); and limiting current 5.53 ± 0.05 nA.[43] These results demonstrated a high correspondence of the regression model to the voltammograms at microelectrodes and the high precision of parameters made possible because of an excellent S/N.

The model for moderately slow or quasireversible electron transfer was used to analyze data for the oxidation of ferrocyanide in 0.5 *M* KNO_3 (pH 6.3) at carbon disk microelectrodes. The following equation was used:

$$i = i_l/(1 + \theta + k'\theta') + mE + i' \qquad (33)$$

where θ has the definition in Equation 9, $\theta' = \exp[(E-E^{o\prime})/S'']$, $S'' = RT/\alpha F$, and $k' = k_m/k^o$, where k_m is a mass transport constant depending on the geometry of the electrode. The equation is written for reductions, but was converted for oxidations by the appropriate changes in sign. For a disk microelectrode, k_m is approximately $(D^o/r)[2/\pi + 3\pi/16]$.[42,43] Excellent fits were obtained using $E^{o\prime}$, k', S'', and i_l as parameters. Values of $E^{o\prime}$ = 430 ± 4 mV vs. NHE (cf. 448 mV on activated glassy carbon) and apparent k^o = 0.023 ± 0.008 cm s^{-1} were obtained on electrochemically treated carbon fiber microelectrodes. The latter value, although approximate because of the necessity of using an approximate k_m, was similar to that[45] of 0.03 cm s^{-1} reported for electrochemically treated glassy carbon in 2 *M* KCl. When the previously discussed data for ferrocene were analyzed by the model in Equation 33, nearly identical average values for limiting current, $E^{o\prime}$, and RT/F were obtained as from regression onto Equation 10, the reversible model. This is expected since the reversible model is a special case of the more general quasireversible model. An apparent k^o for ferrocene of 1 to 2 cm s^{-1} was found, which is close to the upper limit that can be estimated by this method for data with good S/N. The model in Equation 33 can be used for other electrode geometries such as rings or cylinders, for which more exact formulations of k_m are available.[43]

Another application studied for microelectrodes was the estimation of uncompensated resistance (R_u) of the electrochemical cell containing highly resistive solvents. High cell resistance can cause distortion by broadening of i-E curves in voltammetry. Even with modern three-electrode potentiostats, part of this resistance remains uncompensated. External electronic compensation is difficult because of the large cell resistances involved. Although the dependence of ohmic drop on potential in a microelectrode cell is complex, the following approximate relationship between applied voltage V and the actual potential E at the working electrode should hold when ohmic drop is not too large:

$$E = V + iR_u \qquad (34)$$

Combining Equation 34 with Equation 10 with $E' = 0$ yields:

$$i = i_l/[1 + \exp\{(V + iR_u - E^{o\prime})/S'\}] + mE + i' \qquad (35)$$

A similar expression was used successfully for cells containing

dropping mercury electrodes with externally added resistance.[16] To avoid possible under- or overflow during the approach of the regression analysis to convergence, the following conditions were included in the model subroutine:

$$\text{If} \quad (E - E^{o\prime})/S' \leq -10 \quad \text{then} \quad i = i_l + mE + i'$$

$$\text{If} \quad (E - E^{o\prime})/S' \geq +10 \quad \text{then} \quad i = mE + i'$$

This model was tested with i-E data for the reversible oxidation of ferrocene at a carbon disk microelectrode in acetonitrile without added supporting electrolyte. The value of S′ was fixed at RT/F for the reversible reaction and R_u, $E_{1/2}$, i_l, m, and i′ were used as regression parameters. In this case, a modified steepest descent program[2] gave much better convergence than the Marquardt routine, possibly because of partial correlations among background parameters.[43] Analysis of ten voltammograms at scan rates ≤ 10 mV s^{-1} gave an average R_u of 3.47 $\pm$ 0.20 $\times$ 10^6 Ω. A typical set of data (Figure 10) shows goodness of fit of the regression and a "resistance free" voltammogram computed from the best values of the regression parameters by using Equation 10.

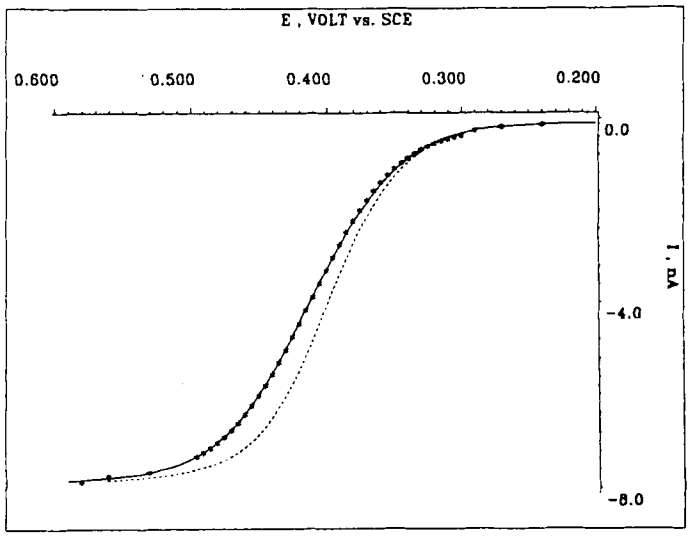

FIGURE 10. Steady-state voltammogram at a carbon disk microelectrode of 6-μm radius for oxidation of 1 m*M* ferrocene in acetonitrile with no added supporting electrolyte. Solid line is experimental data with points computed from nonlinear regression onto Equation 35. Dashed line was computed after removal of estimated ohmic drop.

B. Square-Wave Voltammetry (SWV)

Modern pulse voltammetric methods provide improved sensitivity and resolution over the more traditional linear scan methods. SWV superimposes a square wave of frequency f on a linearly varying potential ramp applied to the working electrode.[46] Currents are measured near the end of each forward and reverse pulse at times when the Faradaic current due to electron transfer is significantly greater than the more rapidly decaying charging current. The two measured currents are subtracted at each cycle of pulses to give difference currents, which are displayed vs. the ramp potential E. The difference i-E curve is generally symmetric and peak shaped.

As in LSV at conventional-sized electrodes, closed-form equations are rarely available for even the simplest electrode reactions in SWV. Therefore, numerical methods must be used to construct regression models for the i-E curves. With the availability of suitable numerical models, nonlinear regression analysis of square-wave voltammograms can provide accurate kinetic parameters in a significantly lower concentration range than is possible with LSV.

A general procedure has been developed for nonlinear regression analysis of square-wave and other types of pulse voltammograms in near real time.[47] The method requires the availability of a dimensionless current function ψ describing a normalized i-E curve for the electrode reaction of interest. The computed ψ's were obtained by numerical integration of the relevant integral equation obtained by an implicit finite difference method. In principle, explicit finite difference models similar to those described in Section III.D could also be used. For use in optimization, the measured difference current i was expressed[47] as:

$$i = a\psi + c + e \qquad (36)$$

where a is a normalization constant, c is a constant background current, and e is normally distributed error. The ψ is a function of system parameters, such as the standard potential, heterogeneous and homogeneous rate constants, and diffusion coefficients. If the model is exact, optimal values of the parameters will give a correlation coefficient (r) of 1.000 in a linear regression of i against ψ (Equation 36). Of course, in the presence of random error, r will be <1. For analysis of square-wave voltammetric data, the quantity (1-r) was minimized by the modified simplex algorithm to determine optimal system parameters. This procedure was shown to be equivalent to the usual nonlinear least-squares minimization. At each vertex in the simplex, a, c, and r are evaluated by the linear regression, so that only the parameter space of the system need be explored. Thus, the optimization is independent of a and c. Although the model is expressed in dimensionless quantities, normalization of currents is not required. A method of estimating confidence intervals for the computed parameters was also described. The reader is referred to the original literature for further computational and statistical details.[46-48]

The above-mentioned method was tested by analysis of SWV data for the two-electron reduction of Zn^{2+} to Zn(Hg), a system exhibiting slow heterogeneous electron transfer. Since the potential of the working electrode depends explicitly on time, ψ is a function of (t, α, κ, $E_{1/2}$). The heterogeneous rate parameter κ is a function of k^o, α, and the diffusion coefficients of Zn^{2+} and Zn(Hg). Thus, analogous to steady-state

voltammetry, nonlinear regression analysis of SWV provides simultaneous estimates of $E_{1/2}$, α, and k° for quasireversible electron transfer at the electrode. Random residual plots and kinetic parameters of excellent precision and accuracy were found for the $Zn^{2+}/Zn(Hg)$ system, even in the micromolar concentration range.[46] Computed parameters and their 95% confidence intervals were $E_{1/2} = -1.0124$ V (± 0.0004); $\alpha = 0.257(+0.010, -0.008)$; $\kappa = 1.295$ $s^{-1/2}$ ($+0.056$, -0.043). Results of good precision and accuracy were also obtained when applying this approach to estimate the pseudo-first-order rate constant for catalytic reductions[46] of a type similar to that in Equations 12 and 13.

C. Linear Sweep Voltammetry — Two-Electron Electrocatalysis

A general method for regression analysis of linear sweep voltammograms has also been developed.[4] It employs expanded space grid digital simulation (Section III.D) to construct models for the i-E curves. The parameters of the model were optimized by using the Marquardt algorithm. As in the method for SWV, normalization of the measured current is avoided. The model computes the current in the dimensions of the experiment. Normalization of the data is unnecessary since the parameters are computed in the regression analysis with their correct dimensions and units. A linear background term was included in the models. The method was tested for the reversible one-electron transfer reactions of several aromatic hydrocarbons in *N,N*-dimethylformamide (DMF). For these reversible one-electron transfer reactions, the relevant parameters are the diffusion coefficient (D) and standard potential (E°). Average results for six sets of data (N = 6) for reduction of 9,10-diphenylanthracene at a spherical mercury electrode were $D = 7.19 \pm 0.47 \times 10^{-6}$ cm^2 s^{-1} and $E^\circ = -1.822 \pm 0.002$ V vs. SCE. (The values are given with their SDs.) These results are excellent considering a $\pm 5\%$ reproducibility of electrode area reflected in the SD of D and small drifts in the potential of the nonaqueous reference electrode. The results agreed well with conventionally measured values of $7.9 \pm 1.2 \times 10^{-6}$ cm^2 s^{-1} and $E^\circ = -1.829 \pm 0.005$ V (N = 51, cyclic voltammetry), and $D = 6.9 \pm 0.9 \times 10^{-6}$ cm^2 s^{-1} (N = 12, chronocoulometry).[4] The method can also be applied to slow electron transfer reactions by fixing E° and using k° and D as regression parameters.

A more demanding application for nonlinear regression of LSV data was elucidation of the rate-determining step (rds) in two-electron electrocatalytic reduction of monohalobiphenyls. This provides an example of the use of nonlinear regression analysis for distinguishing between closely related models for chemical behavior. To illustrate, we consider the mechanism for two-electron electrocatalytic reduction of aryl halides with organic catalysts:

$$A + e = A^{\cdot -} \quad (37)$$

$$ArX + A^{\cdot -} \underset{k_2}{\overset{k_1}{=}} ArX^{\cdot -} + A \quad (38)$$

$$ArX^{\cdot -} \xrightarrow{k} Ar\cdot + X^- \quad (39)$$

$$Ar\cdot + A^{\cdot -} \rightarrow A + Ar^- \quad (40)$$

$$Ar^- + (H^+) \rightarrow ArH \quad (41)$$

Scheme I

The first step is the rapid transfer of an electron from electrode to catalyst A (Equation 37), yielding the anion radical of the catalyst. The rds of the reaction can be either homogeneous electron transfer from the anion radical of the catalyst to halobiphenyl ArX (Equation 38), or cleavage of the anion radical of the halobiphenyl in Equation 39. Subsequently, several fast and kinetically invisible electron transfer and/or chemical steps, represented by Equations 40 and 41, yield the final hydrocarbon product. In LSV experiments on systems following Scheme I, an increase in cathodic current for the reduction of the catalyst occurs upon addition of substrate because of recycling of A at the electrode.

A general digital simulation model (KG model) of the form $i = f(D, E^\circ, k_1, k_2, E)$ featuring second-order kinetics of Equation 38 was developed[5] to describe the shapes of catalytic LSV curves resulting from Scheme I. However, nonlinear regression of simulated data falling under limiting conditions where either Equation 38 with rate constant k_1 (KE case) or Equation 39 (KC case) are rate determining led to severe correlation between the rate parameters. For practical kinetic analysis of the i-E data, it was necessary to evaluate models for the general or mixed kinetic case (KG) and for the two limiting cases.[5] The KE model used the parameters E°, D, and k_1, while the KC model employed E°, D, and the product k_1k_2 as parameters. Tests on computer-simulated data with randomly distributed absolute noise at 0.5% of the peak current, a noise level typical in electrochemical kinetic studies, showed that the three kinetic stiuations could be readily distinguished by nonlinear regression analysis. Criteria used for discrimination were comparison of deviation plots, χ^2 of the residuals, and RSD of the regression. For the noisy simulated data, deviation plots were always random for the correct mechanism. Distinctly nonrandom deviation plots were found for fits of incorrect models onto simulated data.

The method was applied to the electrocatalytic dehalogenations of 4-chloro- and 4-bromobiphenyl (4-CB and 4-BB) with phenanthradine as an electrocatalyst on a spherical mercury electrode in *N,N*-dimethylformamide (DMF). Data were evaluated by regressions in the order: (1) KC model; (2) KE model; (3) KG model. This sequence was followed to avoid

correlations in fits of the KG model to experimental data falling into one of the limiting cases. Deviation plots for the KE models were more random, and the KG model required an excessive number of cycles without convergence. Statistical criteria confirmed the hypothesis that the KE model was correct. Thus, the homogeneous electron transfer in Equation 38 was found to be the rds in both cases. The χ^2 statistic seemed a more discriminating parameter for distinguishing between the closely related models in this application. A graphical illustration of results, including the computed voltammogram of the catalyst, is shown in Figure 11. The rate constants (k_1) found were 1.42 ± 0.12 × 10^3 M^{-1} s^{-1} for 4-CB (N = 6) and 5.1 ± 1.8 M^{-1} s^{-1} for 4-BB (N = 8). Both values were of considerably better precision than rate constants for the same systems found under pseudo-first-order conditions, where the catalytic current had to be extracted from large currents for direct reduction of excess halobiphenyl substrate. Precision for the 4-BB system was lower because of a small residual interference for direct 4-BB reduction which was not accounted for in the model

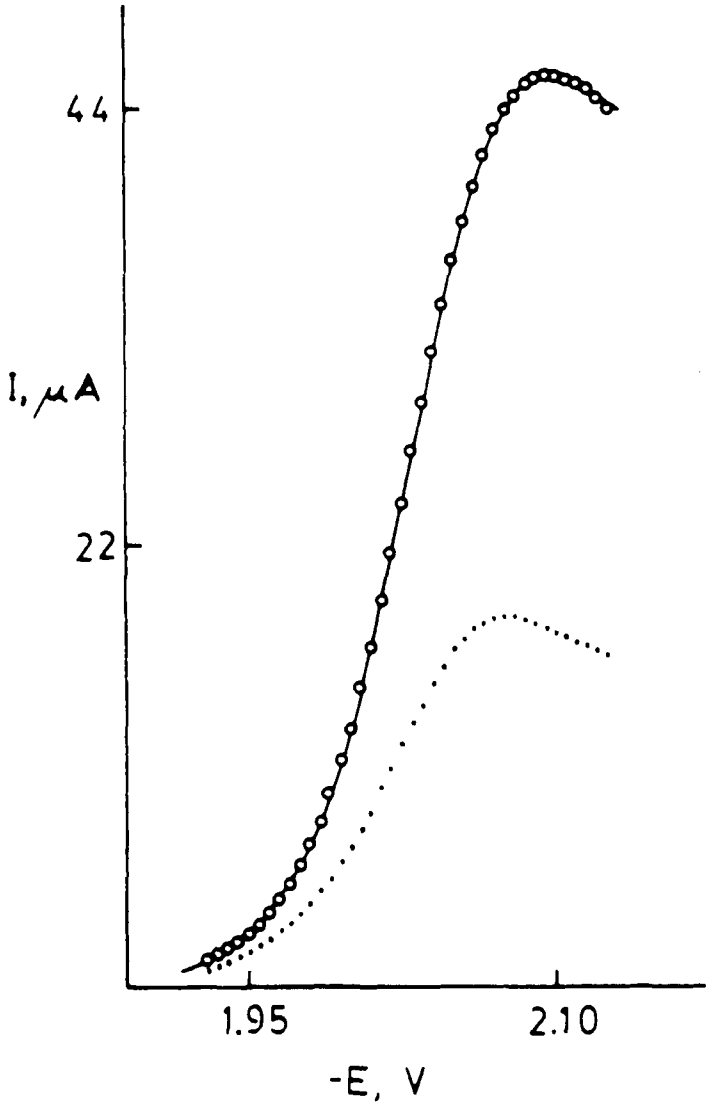

FIGURE 11. Linear sweep voltammogram at a hanging drop mercury electrode for 0.87 m*M* phenanthridine in 0.1 *M* TBAI/DMF at 0.50 V s^{-1}. Solid line is best fit by simulation/regression method (KE model); circles are experimental data. Dotted line is computed LSV for phenanthridine alone. (Reprinted from Arena, J. A. and Rusling, J. F., *J. Phys. Chem.*, 91, 3368, 1987. With permission. Copyright 1987. American Chemical Society.)

The inclusion of second-order kinetics in the model allowed estimation of higher rate constants than possible under pseudo-first-order conditions. This is because nearly equal concentrations of catalyst and substrate could be used, thereby minimizing the rate of the reaction. The second order strategy avoids rate saturation for very fast reactions, i.e., it allows experiments to be done under experimental conditions where the catalytic current is a sensitive indicator of reaction rate. Second-order conditions also minimize contributions to the current from direct reduction of substrate.[18] For electrocatalytic systems where substrate is reduced at potentials very much more negative than the E° of the catalyst, the upper limit of k_1 is much larger than the value found for the 4-BB system. In the electrocatalytic reduction of 1,2-dibromobutane to butene by vitamin B_{12r}, reduction of substrate occurs at 0.8 V more negative than that of the Co(II)/Co(I) catalyst. Here, the digital simulation/regression method gave k_1 = 6.1 ± 2.2 × 10^6 M^{-1} s^{-1}. It was predicted that values at least tenfold larger could be estimated by this method.[5] The simulation model for this vitamin B_{12} catalysis required minor modifications to include unequal diffusion coefficients of substrate and catalyst, planar diffusion, and smaller values of the heterogeneous rate constant of the catalyst.[6] The modifications are easily accommodated within the general simulation model.

D. Chronocoulometry — Linear vs. Nonlinear Regression

In this electrochemical method, a single or double step of potential is applied at working electrode and the accumulated charge passing through the cell is recorded vs. time. In a typical double-potential-step chronocoulometric experiment, the potential at the working electrode is first held at an initial potential (E_i) where no electrolysis takes place. At t = 0, the potential is rapidly stepped to a value (E_f) at which the desired electrode reaction takes place at a diffusion-limited rate. At t = τ, with τ ranging from a few milliseconds to several seconds, the potential is returned to E_i. The charge (Q) passing through the electrochemical cell is measured vs. t over the period 0 to 2τ (Figure 12).

Double-potential step chronocoulometry has been applied extensively to investigate adsorption of electroactive molecules and ions[49-52] and for measuring rate constants of chemical reactions coupled to heterogeneous electron transfer reactions.[52,53] A particular advantage of the method is that the amount of electricity needed to charge the electrode double layer can be separated easily from Faradaic charge from electrolysis of adsorbed and soluble species.The advantage

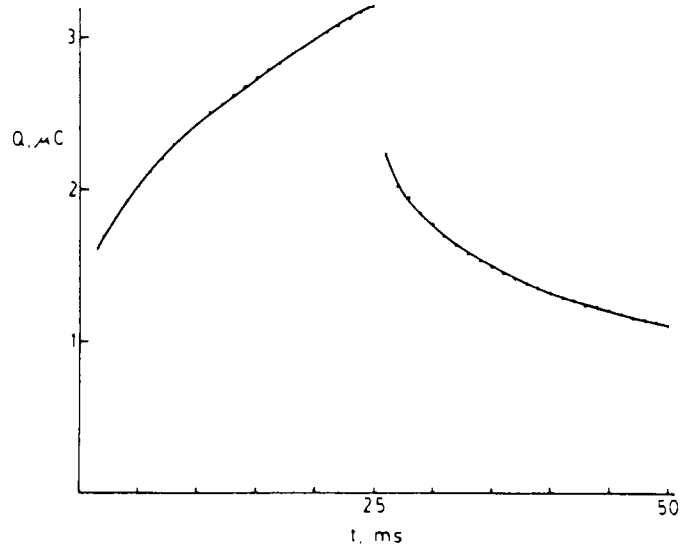

FIGURE 12. Chronocoulometry of 1 m*M* Cd(II) in 0.8 *M* $NaNO_3$/0.2 *M* KSCN at $\tau = 0.025$ s. Points are experimental data; solid line computed from nonlinear regression onto Equations 44 and 45. (Reprinted from Rusling, J. F. and Brooks, M. Y., *Anal. Chem.*, 56, 2147, 1984. With permission. Copyright 1984, American Chemical Society.)

results because it is the Faradaic charge which provides information about the redox processes taking place during the electrode reaction. Chronocoulometry is a sensitive indicator of adsorption and can be used to measure surface concentrations, even at low surfaces coverages for weakly adsorbed electroactive species.

One way of analyzing chronocoulometric data for electrochemical processes involving electron transfer uncomplicated by chemical steps is by using approximate linear forms of the Q vs. t equations. This analysis assumes that plots of $Q(t<\tau)$ vs. $t^{1/2}$ and $-Q_r = Q(t > \tau)$ vs. T', where $T' = \tau^{1/2} + (t - \tau)^{1/2} - t^{1/2}$, are linear and that double layer charging and electrolysis of adsorbed reactant are very fast with respect to the time width of the potential pulse. The linearized model is based on semi-infinite linear diffusion at a planar electrode. As pointed out by the originators of the method,[49,50] this assumption is reasonable at small τ, but may lead to considerable error as τ is increased. In the discussion that follows, nonlinear regression of Q vs. t data onto the relevant equations in the form $Q = f(t)$ is compared with linear regression analysis of data using the approximate linearized expressions.

First, consider the simple one electron transfer reaction in Equation 8, where both O and R are soluble and only O is initially present in the solution at a concentration C_o^*. Under conditions of the chronocoulometic experiment at a spherical electrode such that $E_i >> E^{o'}$ and $E_f << E^{o'}$, the following equations for the discontinuous Q-t curve are obtained:[54]

$$Q_1(t < \tau) = 2nFAD_o^{1/2}C_o^*\pi^{-1/2}[t^{1/2} + b_1\pi^{1/2}D_o^{1/2}t/2r] + Q_{dl} \quad (42)$$

and for the reverse step:

$$Q_1(t > \tau) = 2nFAD_o^{1/2}C_o^*\pi^{-1/2}[t^{1/2} - (t - \tau)^{1/2} + b_1\pi^{1/2}D_o^{1/2}\tau/2r + b_2\pi^{1/2}D_r^{1/2}(\tau - t)/2r] \quad (43)$$

where n is the number of electrons transferred per electroactive molecule or ion, A is the electrode area, D_o and D_r are diffusion coefficients of O and R, r is the radius of the electrode, b_1 and b_2 are empirical constants multiplying spherical correction terms, and Q_{dl} is the charge required for reorganizing the electrode double layer after each step in potential. Terms containing r account for electrode geometry. In this case, they provide the so-called spherical correction, but similar expressions can be used for edge effects at planar electrodes. The constants b_1 and b_2 are predicted to be close to one when O and R (Equation 8) are both soluble in the solution.[55] These constants will differ when R forms an amalgam with a mercury electrode.

Equations 42 and 43 were used for simultaneous nonlinear regression analysis of the two branches of the chronocoulometric curves by using four parameters:

$$2nFAD_o^{1/2}C_o^*\pi^{-1/2},\ b_1\pi^{1/2}D_o^{1/2}/2r,\ b_2\pi^{1/2}D_r^{1/2}/2r,\ \text{and}\ Q_{dl}$$

In the linear plot method, correction terms for electrode geometry are neglected because of their nonlinear contribution. $Q(t < \tau)$ is plotted vs. $t^{1/2}$ as is $-Q_r$ vs. T', where $T' = \tau^{1/2} + (t - \tau)^{1/2} - t^{1/2}$. The two plots are approximately linear with equal slopes of $S' = 2nFAD_o^{1/2}C_o^*\pi^{-1/2}$ and have intercepts with the Q-axis of opposite sign and equal to Q_{dl}. Thus, the experimental slopes, which can be computed by linear regression, are used to obtain D_o. The intercepts should be equal in the absence of adsorption and give two measures of Q_{dl}. The latter values should be equal to one another.

Nonlinear regression onto Equations 42 and 43 for data for the one electron reductions of Tl(I) and U(VI) in 0.1 *M* HCl at spherical hanging drop mercury electrodes was compared to analysis of the same data by the linearized equations.[54] A total of 24 sets of data were collected for each system, with τ ranging from 25 to 500 ms. One data point per millisecond was acquired. For the linear plot analyses, all the data points in a given set were analyzed by using linear regression. For the nonlinear regression analyses, 50 data points equally spaced on the time axis were analyzed. Mean values of D and Q_{dl} computed by nonlinear regression of the Tl(I) and U(VI) data were in reasonable agreement with those obtained by the linear plot method, but agreement with independently measured D values was slightly better for the nonlinear regression method. No significant differences in precision were observed for the results from the two different ways of analyzing the data. However, an increase in τ caused an increase in the differences between positive and negative intercepts of the Q-axis in the linear plots. These values do not remain equal (as assumed in the linearized model) at higher τ because of the increased importance of

spherical corrections at longer times. To the unwary experimentalist, such a variation from the expected behavior of the linear model could lead to incorrect interpretations.

Analysis of data for systems with reactant (O) adsorbed was also studied by the above approach.[54] Assuming that Γ_o mol/cm^2 of O is initially adsorbed to the electrode and reacts instantaneously at the time of the first potential step, the model is based on the following reactions occurring at the electrode:

$$O(ads) + ne = R$$
$$O + ne = R$$

Here, the first equation expresses reduction of adsorbed O, while the second represents reduction of O diffusing to the electrode from the bulk solution. The following equations for the discontinuous response curve are obtained:

$$Q(t < \tau) = Q_1(t < \tau) + nFA\Gamma_o + Q_{dl} \quad (44)$$

$$Q(t > \tau) = Q_1(t > \tau) + nFA\Gamma_o[(2/\pi)\sin^{-1}(\tau/t)^{1/2}] \quad (45)$$

where the Q_1's are given by Equations 42 and 43. Equations 44 and 45 were used for nonlinear regression employing the same parameters as in the reversible model, except with $Q_{dl} + nFA\Gamma_o$ replacing Q_{dl} on the forward pulse and the addition of a new parameter $nFA\Gamma_o$ in the equation for the reverse pulse. For use in the linear plot, neglecting electrode geometry corrections, the following expression is derived:[50-52]

$$Q_r = 2nFAD_o^{1/2}C_o^*\pi^{-1/2}T' + nFA\Gamma_o[1 - (2/\pi)\sin^{-1}(\tau/t)^{1/2}] + Q_{dl} \quad (46)$$

For linearization of Equation 46, the $[1 - (2/\Pi)\sin^{-1}(\tau/t)^{1/2}]$ term is approximated by the linear function $a_1(T'/\tau^{1/2}) + a_o$. Values of a_o and a_1 are obtained by linear regression of the exact expression onto the linear one. The plot of Q_r vs. T' has an approximate slope of $S_r = (2nFAD_o^{1/2}C_o^*\Pi^{-1/2})(1 + a_1nFA\Gamma_o/Q_c)$, where $Q_c = 2nFAD_o^{1/2}C_o^*\Pi^{-1/2}\tau^{1/2}$. The intercept with the Q-axis is $Q_r^\circ = Q_{dl} + nFA\Gamma_o a_o$. The plot of $Q(t < \tau)$ vs. $t^{1/2}$ has slope S' and intercept $Q^\circ = Q_{dl} + nFA\Gamma_o$. The surface concentration of adsorbed O is obtained from:

$$nFA\Gamma_o = (Q^\circ - Q_r^\circ)/(1 - a_o) \quad (47)$$

The slopes of the linear plots are used to find D_o.

The reduction of Cd(II) in aqueous sodium thiocyanate/sodium nitrate solutions was used as the test system to compare the nonlinear and linear regression methods of analyzing the data. Under the experimental conditions used,[54] thiocyanate induces adsorption of Cd(II), and both adsorbed and diffusing Cd(II) are reduced at the electrode. Nonlinear regression of 50 data points equally spaced on the t-axis onto Equations 44 and 45 gave excellent results for D and Γ_o for data with $\tau < 100$ ms, but a systematic error in Γ_o was found for data at longer times. A quantitative study of the errors in surface concentration created by errors in measured charge along the time axis was done by pointwise variance analysis.[1] This technique provided standard errors of all parameters and also showed how relative weights in determining Γ_o (or any parameter) depended on t (Figure 13). These results showed that standard error in Γ_o increased as τ increased when data equally spaced on the t-axis were analyzed. Since the reduction of adsorbed O is assumed to occur very rapidly upon application of the forward potential pulse, most of the information about surface concentration is contained just after $t = 0$ and again on the reoxidation or reverse pulse just after $t = \tau$.

The relative weight plot (Figure 13) suggested that better values of Γ_o could be obtained by choosing the data points to be analyzed in time zones just after the beginning of the experiment and in a time range 25% of τ before and after $t = \tau$. In this strategy, data are no longer equally spaced on the t-axis, but are grouped or clustered in the time regions where they give the largest weight or contribution to the computed surface concentration. In other words, only data points containing significant information about the surface concentration are analyzed. By using this point-clustering strategy, good values of Γ_o close to the previously reported value were obtained (Table 3). Precision and accuracy from the nonlinear regression analysis was significantly improved over the approximate linear plot method, especially at longer τ.[54] This illustrates intuitive optimization of a clustered data set. A systematic method based on relative weight plots to find

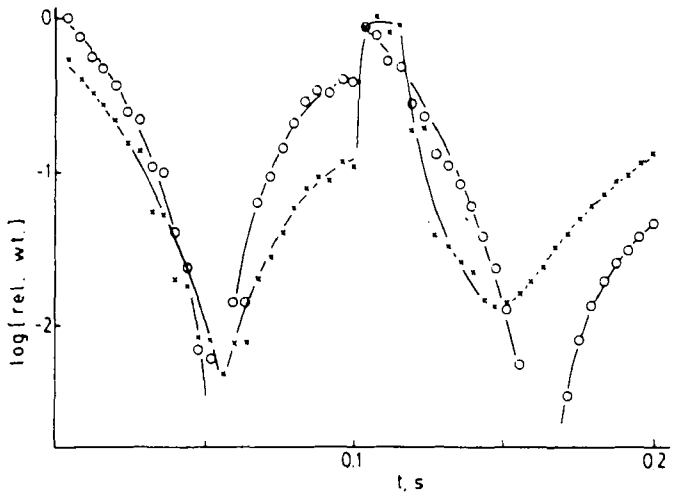

FIGURE 13. Pointwise variance analysis for theoretical data for a chronocoulometric experiment with reactant adsorption (Equations 44 and 45). The plot shows how relative weights in determining $nF\Gamma_o$ (O) and overall relative weights (X) vary with t for $\tau = 0.10$ s (Reprinted from Rusling, J. F. and Brooks, M. Y., *Anal. Chem.*, 56, 2147, 1984. With permission. Copyright 1984, American Chemical Society.)

Table 3
Parameters for Data on Cd(II)/SCN⁻ on a Mercury Electrode Analyzed by Nonlinear Regression (Equations 44 and 45) and Linear Plot Methods[a]

τ (ms)	N[b]	10^5D (cm²/s)		Q_{dl} (μC)		$nF\Gamma_o$ (μC/cm²)	
		NLR	Linear	NLR	Linear	NLR	Linear
25	14	0.87 ± 0.03	0.88 ± 0.03	0.57 ± 0.04	0.52 ± 0.07	24.2 ± 1.1	26.3 ± 2.5
100	8	0.74 ± 0.03	0.75 ± 0.03	0.55 ± 0.07	0.65 ± 0.07	23.7 ± 2.1	21.2 ± 2.9
500	5	0.74 ± 0.01	0.74 ± 0.01	0.69 ± 0.04	0.75 ± 0.04	21.7 ± 0.8	18.1 ± 1.9

[a] 0.5 m*M* Cd(II) in 0.8 *M* $NaNO_3$/0.2 *M* KSCN. All data (one Q per millisecond) were used for linear regressions, but data for NLR were grouped in regions of highest significance (see text). Previous results from Reference 50 were D = 0.74 × 10^5 cm²/s and $nF\Gamma_o$ = 21.1 μC/cm² by linear plot method.

[b] No. of data sets analyzed.

the data set which maximizes precision of parameters was recently published.[56]

Errors in the linear plot method were investigated by using noise-free simulated data computed from Equations 44 and 45. Systematic high biases of 5 and 8%, respectively, were found in surface concentrations computed from linear regression intercepts at pulse widths of 25 and 100 ms. The number of data analyzed in each set was twice the pulse width in milliseconds.

A characteristic deviation pattern was found when chronocoulometric data representing reactant adsorption were fitted to the equations for a pure diffusion-controlled system. Thus, fitting an unknown set of experimental data to Equations 42 and 43 can be used as a diagnostic test for adsorption. Observation of a deviation plot of the characteristic shape (Figure 14) suggests the reactant adsorption model. Reactant adsorption can then be confirmed by subsequently fitting clustered data to Equations 45 and 46 for this case and observing a random deviation plot.[54] The latter regression provides reliable values for the diffusion coefficient and the surface concentration of reactant.

A similar approach to that described here was used, with the appropriate models, to study the kinetics of chemical reactions occurring between two electron transfer steps.[53] Electrochemists call this type of electrode reaction an ECE (electron transfer - chemical step - electron transfer) reaction. To determine the rate constant of the chemical step for ECE reactions, only the forward pulse Q-t data need to be analyzed. The optimum time range for data collection for precise estimations of rate constants were identified with pointwise variance analysis. In applications to the oxidative hydroxylation of tetrahydrocarbazoles, it was found that carbon paste electrodes gave data with a small enough background charge to be used directly. Platinum and glassy carbon electrodes had large background charges and the data were difficult to use directly for nonlinear regression. Separately measured background charge can be subtracted from the data if it is reproducible and can be measured accurately. The corrected Q-t data should be regressed onto a model including Q_{dl} since this quantity may be different in the presence and absence of the electroactive species if any adsorption is involved. In general, redox processes occurring on the surface of solid electrodes are likely to contribute to the measured charge. Failure to realize and compensate for such contributions can lead to large errors in the parameters obtained from regression analyses.

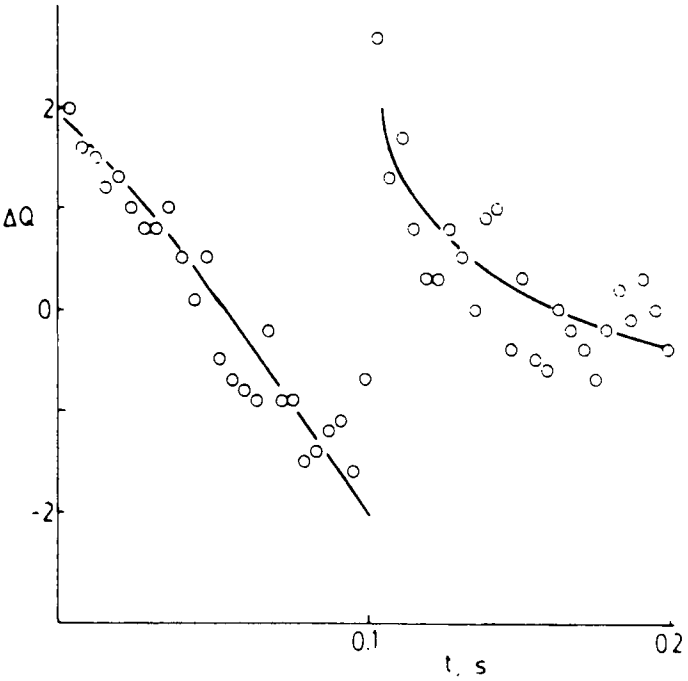

FIGURE 14. Deviation pattern recognition test for reactant adsorption. Solid line is theoretical deviation pattern for noise-free chronocoulometric data for reactant adsorption (Equations 44 and 45) fit to the model for a diffusion controlled reaction (Equations 42 and 43). Circles represent the deviation plot from experimental data for 1 m*M* Cd(II) in 0.8 *M* $NaNO_3$/0.2 *M* KSCN regressed onto the diffusion model. (Reprinted from Rusling, J. F. and Brooks, M. Y., *Anal. Chem.*, 56, 2147, 1984. With permission. Copyright 1984, American Chemical Society.)

E. Multiple Equilibria

Many types of experimental data in physical and biological

science can be analyzed with models based on the binding equilibria of small molecules or ions to macromolecules, molecular aggregates, colloids, or surfaces containing multiple binding sites. A classical example from physical biochemistry is the binding of small ions or molecules to proteins or nucleic acids. Other studies for which such an approach may prove fruitful are solubilization of small ions or molecules by molecular aggregates such as micelles and microemulsions and adsorption of molecules or ions on colloidal particles or bulk solids. The nucleus of a general approach to such problems based on the law of mass action was outlined more than 20 years ago by Wyman in his principle of linked functions.[29] His approach allows an experimentally observed quantity to be modeled in terms of the multiple equilibria involved. This "thermodynamic linkage" method has been coupled with nonlinear regression analysis in recent applications to a number of biochemical problems by Farrell and Kumosinski.[57] The rationale and framework of the approach are presented here in a general way, followed by a discussion of several applications.

Equilibria for binding of an ion or molecule X to a macromolecule M with n binding sites can be represented as:

$$M + iX = MX_i; \qquad i = 1 \text{ to } n \tag{48}$$

Apparent equilibrium constants for the n reactions are given by:

$$K_i = [MX_i]/\{[M][X]^i\} \tag{49}$$

As n becomes large, so does the number of equilibria and equilibrium constants needed to describe the system. The problem quickly becomes unmanageable in a practical sense, especially as n climbs toward double-digit integers. If two separate species X and Y can bind to M, a situation not uncommon in macromolecular chemistry, a large number of binding sites make an exact thermodynamic description of the system nearly impossible.

An alternative representation presented by Tanford[28] was used by Farrell and Kumosinski[57] to simplify multiple equilibrium models for nonlinear regression analysis. In the simplest case where all binding sites can be considered equivalent, Tanford suggested relating the n K_i's for the reactions in Equation 48 to an apparent equilibrium constant (K') per binding site. Equations 48 and 49 are then rewritten as:

$$M + nX = MX_n \tag{50}$$

$$K'^n = [MX_n]/\{[M][X]^n\} \tag{51}$$

This is analogous to the practice of treating multiple metal-ligand equilibria with an overall equilibrium constant which is the product of all the equilibrium constants for the individual steps. In our example, $K'^n = K_1K_2. \ldots .K_n$.

Now suppose there is a characteristic measurable quantity (P') depending on the properties of M and MX_n and which can be expressed as:

$$P' = f_M P_o + f_{MXn} P_1 \tag{52}$$

where f_M and f_{MXn} are the (mole) fractions of M in the free and bound forms, P_o is the value of the measured property characteristic of M, and P_1 is the value of that property characteristic of MX_n. On the other hand, if P' depends on the properties of the "probe" species X, we have:

$$P' = f_a P_o + f_b P_1 \tag{53}$$

where f_a and f_b are the fractions of unbound and bound X, respectively. P_o and P_1 in Equation 53 refer to characteristic properties of free X and the MX_n complex. In both cases, the sum of all the fractions must equal unity. Thus, $f_a = 1 - f_b$, and $f_M = 1 - f_{MXn}$

Working models for P' can be constructed by expressing the fractions of each relevant species in terms of the equilibrium in Equation 50 and K' in Equation 51. It is useful to relate P' to the total concentrations of X (C_X) and M (C_M). Using the symbol x = [X], we have[29]

$$C_X = x + [M]nK'^n x^n \tag{54}$$

$$C_M = [M] + [M]K'^n x^n \tag{55}$$

Then:

$$f_M = [M]/C_M = 1/(1 + K'^n x^n) \tag{56}$$

$$f_{MXn} = K'^n x^n/(1 + K'^n x^n) \tag{57}$$

and

$$f_a = x/C_X = 1/(1 + [M]nK'^n x^{n-1}) \tag{58}$$

$$f_b = [M]nK'^n x^{n-1}/(1 + [M]nK'^n x^{n-1}) \tag{59}$$

Substituting Equations 56 through 59 into Equations 52 and 53 yields the two models for P' expressed as functions of K', [M], and x. Simplifying assumptions and approximations can often be made such that the total concentrations of M and X, which are usually known, appear in the models rather than [M] and x. For example, suppose we measure the quantity P' which is dependent on the properties of the macromolecule. Starting from Equation 52, and substituting for the mole fractions from Equations 56 and 57, the model now becomes:

$$P' = P_o/(1 + K'^n x^n) + P_1 K'^n x^n/(1 + K'^n x^n) \tag{60}$$

If the experiments can be done under conditions where $C_X >> C_M$, and the total number of binding sites in the system is much smaller than C_X, then nearly all the X remains unbound and x = C_X. The expression for P′ can now be written:

$$P' = P_o/(1 + K'^nC_X^n) + P_1K'^nC_X^n/(1 + K'^nC_X^n) \quad (61)$$

This model has the advantage that it is independent of the concentration of M and depends on the known total concentration of X and on K′.

Equation 61 is suitable for nonlinear regression analysis of experimental P′ vs. C_X data. The regression parameters are K′, P_o, and P_1. The usual way of approaching the problem is to do the nonlinear regressions with fixed n and to increase n by one in each successive regression analysis until a clear minimum in the standard deviation of regression is found. Models involving more complex equilibria influencing P′ can be developed in an analogous way.

This approach to modeling was applied by Farrell and Kumosinski[57] to data on the salting in and salting out of proteins. Solubility data on caseins at a series of salt concentrations were analyzed. The best fit was found for a model assuming two classes of binding sites for the ions responsible for the sequential precipitation (salting out) and resolubilization (salting in) of the caseins. The equilibria involved were formulated as:

$$M + nX \overset{K_1^n}{=} MX_n + mX \overset{K_2^m}{=} MX_nX_m$$

where n and m are the number of moles of X bound to the two sites, and K_1 and K_2 are the apparent binding constants per site. The measured quantity was apparent protein solubility S′. Defining S_o, S_1, and S_2 as the intrinsic solubilities of M, MX_n, and MX_nX_m, respectively, the model for S′ has the form:

$$S' = f_MS_o + f_{MXn}S_1 + f_{MXnXm}S_2 \quad (62)$$

By expressing the fractional components in terms of the above equilibria and making the assumption that x = C_X at high relative concentration of salt, the following model was formulated:

$$S' = S_o/(1 + K_1^nC_X^n) + S_1K_1^nC_X^n/(1 + K_1^nC_X^n) + (S_2 - S_1)K_2^mC_X^m/(1 + K_2^mC_X^m) \quad (63)$$

This model represents sequential binding.[57] That is, $K_1 < K_2$ and the n sites become saturated with X prior to significant binding of X to the m sites. In a way similar to the recommended use of Equation 61, Equation 63 was used for nonlinear regression analysis of S′ vs. C_X data for proteins by using S_o, S_1, S_2, K_1, and K_2 as parameters with fixed values of n and m. Successive regression analyses were done with a series of new fixed integer values of n and m until the n and m values were found which gave the minimum standard deviation of the regression.

The model in Equation 63 was applied to the calcium-ion-induced solubility of several types of the protein casein and its genetic variants. Equation 63 provided good descriptions of the data for experimental conditions under which only salting out occurred as well as those under which both salting out and salting in were observed as the concentration of calcium ion was increased. An example of the results for a system following the latter type of behavior is given in Figure 15. Solubility profiles induced by other divalent cations also gave fits of excellent quality. Results implicated participation of the phosphate and carboxylate groups of the proteins in the cation-binding phenomena. The model in Equation 63 was also able to explain similar solubility profiles for proteins from soybeans as the concentration of 1:1 salts were increased.[58]

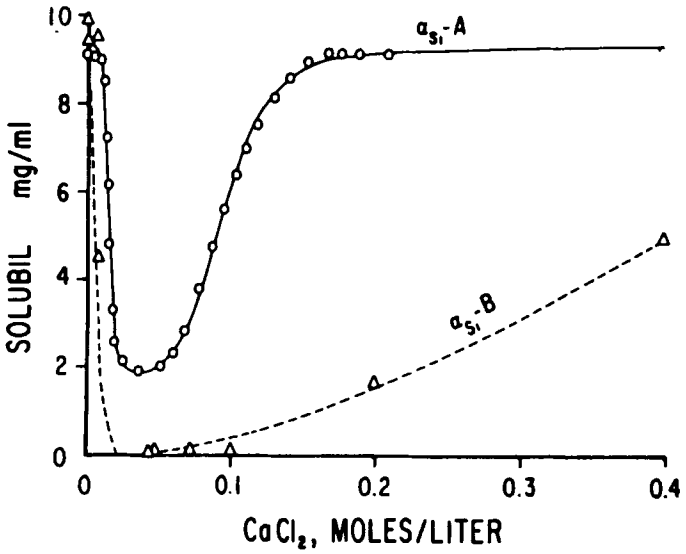

FIGURE 15. Solubility at 1°C of calcium α_{s1}-A and α_{s1}-B caseinates vs. concentration of $CaCl_2$. Solid line represents regression onto Equation 63. (Reprinted from Farrell, H. M. and Kumosinski, T. F., *J. Ind. Microbiol.*, 3, 61, 1988. With permission. Copyright 1988, Elsevier Science Publishers.)

A similar approach was used to model diffusion coefficients of electroactive probe molecules in aqueous micelle solutions.[59] Since the measured diffusion coefficient (D′) is a function of the bound "probe", Equation 53 and its extensions to polydisperse systems was the starting point for the models tested. From these, approximate relationships describing the dependence of the electrochemically measured apparent diffusion coefficient (D′) on concentration (C_X) of a micelle-bound electroactive probe X were derived. Here, the micelle serves as the "macromolecule" in the multiple binding equilibria. In this application, simplifications introduced for the range of experimental conditions possible relegated the per site equilibrium constants to the role of adjustable apparent binding parameters. Models for mono- and polydisperse systems were

applied to systems employing methyl viologen and ferrocene as probes in 0.1 *M* SDS/0.1 *M* NaCl and ferrocene in 0.1 *M* cetyltrimethylammonium bromide (CTAB) with 0.1 *M* NaCl or KBr. Nonlinear regression analysis of D′ vs. C_x data onto the models enabled an assessment of polydispersity and an accurate estimate of micelle diffusion coefficients. The aqueous systems studied were shown to contain two types of micelles of different size. Water-in-oil microemulsions of the surfactant Aerosol OT in water/isooctane were shown to contain one type of inverted micelle-like aggregate by the same method.[60]

Diffusion coefficients of the smaller SDS and CTAB micelles computed from the D′ data were in excellent agreement with values previously obtained by established methods. For example, for 0.1 *M* SDS/0.1 *M* NaCl, the values found for D were 1.41 ± 0.03 and 1.45 ± 0.01 × 10^{-6} cm^2 s^{-1} for methyl viologen and ferrocene probes, respectively. They agree very well with the 1.45 × 10^{-6} cm^2 s^{-1} found for this system by the Taylor dispersion tube method and that of 1.40 × 10^{-1} cm^2 s^{-1} found by quasi-elastic light scattering.[59]

F. Analytical Spectroscopy

The matrix approach (Section II.D) to nonlinear regression was used successfully in several peak resolution problems employing multivariate spectroscopic data. A few of these applications from the work of Harris and co-workers are discussed in this section. Since the data involved more than one dependent variable, the matrix formulation was well suited to organizing and processing the large multicomponent data sets.

1. Multicomponent Time-Resolved Fluorescence Spectra

The addition of time as a second independent variable to fluorescence emission intensity vs. wavelength experiments provided the additional information required to allow resolution of overlapped peaks in the emission spectra.[61] The data consisted of fluorescence spectra of a mixture of n compounds collected at nanosecond time intervals following pulsed photoexcitation. These data were placed in a matrix [D] consisting of w rows, one for each wavelength observed, and t columns corresponding to the number of time intervals. Assuming linear response of the detector with concentration of each of the k independent emitting compounds, elements of the data matrix at wavelength i and time interval j can be expressed as:

$$D_{ij} = \sum_{k=1}^{n} A_{ik}C_{kj} \quad (64)$$

where A_{ik} is the molar emission intensity of compound k at wavelength i and C_{kj} is the concentration of excited state compound k at time interval j. The data matrix was expressed as:

$$[D] = [A][C] \quad (65)$$

Here, [A] is a w × n matrix containing the fluorescence spectra of the n compounds. [C] is a n × t matrix containing the decay of excited state concentrations with time. Resolution of the spectra of the individual components from that of the mixture requires decomposition of the data matrix into [A] and [C]. First-order decay kinetics of all excited states was assumed. A trial matrix [C′] was defined by:

$$C'_{kj} = I_j^* \exp(j\Delta t/\tau_k) \quad (66)$$

where I_j is the measured time response function of the instrument and the asterisk is the convolution integral. There is one parameter per compound, τ_k, its excited state lifetime. Initial guesses of the τ_k's yield an initial [C′]. The best spectral matrix [A′] is obtained from:

$$[A'] = [D][C']^T\{[C'][C']^T\}^{-1} \quad (67)$$

This gives an [A′] which, for a given [C′], minimizes the error sum S expressed in the form of Equation 7. The error sum is essentially the usual sum of squares of deviations between experimental and computed data, where the computed or model data are given by:

$$[D'] = [A'][C'] \quad (68)$$

The regression analysis employed the n lifetimes as parameters and the minimum error sum S was found by the modified simplex method. Since negative elements in [A′] are not physically meaningful, S was multiplied by a function which penalized occurrence of such negative elements during the regression analysis.

The method was evaluated with noisy simulated two-component data and from real samples containing mixtures of two fluorescing compounds. Better precision was found for both lifetimes and preexponential factors when compared with a reiterative convolution of the time decays alone.[61] For the two-component data tested, the number of compounds present could be found by comparing goodness of fit for the series of models with successively increasing integer n values. The n value providing the smallest error sum gave the number of components present.

2. Resolution of Overlapped Chromatographic Peaks

Data obtained from multichannel detection of chromatographic peaks was resolved by procedures similar to those described earlier. Multichannel detection is characteristic of such "hyphenated" techniques as gas chromatography-mass spectrometry (GC-MS), gas chromatography-infrared spectrometry (GC-IR), liquid chromatography-MS, etc.

Following the protocol outlined previously for emission intensity-wavelength-time data, the multichannel detector data was organized in a [D] matrix of x rows and t columns, where x is the number of spectral channels and t is the number of time channels at which the spectra are observed.[62] The time axis corresponds to the elution time of the chromatographic experiment. For resolution of the overlapping chromatographic peaks, the data matrix is decomposed into its component matrices defined by:

$$[D] = [A][Q][C] \quad (69)$$

where [A], of dimensions x × n, contains the normalized spectra of the n compounds represented in the overlapped peak, [Q] is a n × n diagonal matrix representative of the amount of each compound present, and [C] is a n × t matrix containing normalized chromatograms of the n compounds. The resolved chromatographic peaks were modeled as convolutions of Gaussian peak shape with a single-sided exponential to account for tailing. Thus, the elements of the trial [C'] matrix for the kth compound at time j are given by:

$$C_{kj} = G^*_{kj}\exp(j\Delta t/\tau) \quad (70)$$

where * is the convolution integral, Δt is the time between collection of each individual spectrum, and

$$G_{kj} = (t_k/N^{1/2})(2\pi)^{-1/2}\exp\{(j\Delta t - t_k)^2/2(t_k/N^{1/2})^2\} \quad (71)$$

Here, the number of theoretical plates (N) in the chromatographic column and the tailing decay lifetime (τ) are assumed to have been measured on pure samples. Only one parameter per compound, the retention time t_k, was required for the nonlinear regression. Analogous to the use of Equation 67 in the fluorescence example, the best matrix product [A'][Q'] was found from:

$$[A'][Q'] = [D][C']^T\{[C'][C']^T\}^{-1} \quad (72)$$

The error sum minimized in this application was the sum of squares of the residuals between [D] and the model matrix [D'] weighted by the inverse of the degrees of freedom in the regression analysis.[62] The model is given by:

$$[D'] = [A'][Q'][C'] \quad (73)$$

Again, the error sum included a penalty for physically unrealistic negative elements in [A']. The error sum was minimized using the simplex method.

The technique was first evaluated with GC-MS data on two- and three-component mixtures, all of which eluted in a single poorly resolved peak. The number of components (n) was found accurately by successive fits with increasing integer n-values until the minimum error sum showed no further decreases. In most cases, a clear minimum indicated the correct n. The regression technique successfully resolved major components of mixtures having a high degree of overlap in both their chromatograms and mass spectra. However, quantitation of minor components was limited in this initial application because of a slow spectral sampling rate. Nevertheless, the technique avoids some of the pitfalls associated with empirical peak separation routines or those based on library searching or factor analysis.[62]

A second application was made to high-pressure liquid chromatography (HPLC) using a multiple wavelength photodiode array as the multichannel detector.[63] The data matrix was expressed by Equation 65, where [A] contained the chromatograms. Concentration profiles in the rows of [C] were normalized over the total elution volume. The chromatographic peaks were again modeled by convoluting a Gaussian peak shape with an exponential peak tail, as in Equation 70. Fitting of the HPLC peaks required both retention time (t_k) and bandwidth to be used as parameters for each of the n components. The modified simplex method was again used to find the minimum error sum.

The above regression procedure was tested for resolving five- to eight-component mixtures. Successful resolution of overlapped peaks with up to seven components was achieved. Severely overlapped minor components in binary mixtures could be detected at a 95% confidence level when present in amounts above about 35%, depending on peak separation factor and S/N of the data.[63]

Matrix nonlinear regression techniques analogous to those described here have been applied to multiple wavelength data reflecting acid-base equilibria in complex mixtures. Absorption spectra and pK_a values were determined for mixtures of up to four components.[64] A modified method was later reported which included singular value decomposition of the data matrix prior to the nonlinear regression analysis.[65]

V. DEVIATION PATTERN RECOGNITION AND EXPERT SYSTEMS

A. General Concepts

Expert systems attempt to capture in a computer program the problem-solving abilities of a human expert on a given subject. Research into the construction of such software is a subset of the field of artificial intelligence. Expert systems have been developed for a variety of analytical techniques, including interpretation of mass and nuclear magnetic resonance spectra and X-ray powder diffraction spectrometry.[66] Expert systems that automatically and accurately classify chemical data with regard to the type of chemical behavior characteristic of the system would be extremely useful to chemists. Such programs would allow routine decisions about data analysis to be handled by a computer. A straightforward example is the method described in the previous section for resolving individual

components of overlapped chromatographic peaks from multichannel detection data. Generally, the number of components (n) will not be known, but it should be possible to automatically determine n by successive regression analyses by incrementing the value of n by one each time. After "learning" to recognize the required best-fit criteria, such as the minimum error sum in a series of regressions, a computer could automatically decide when the optimum n is reached. This information could then be conveyed to the user along with the best values of the analytical parameters. This example is a very simple one. More complex problems are also amenable to solution by expert systems. Suppose there exists a library of mathematical models for a given type of analytical response curve. An expert system can be based on regression analyses of the response curve onto a systematically selected series of these models until the computer recognizes the best fit in terms of previously "learned" criteria. Information from incorrect fits could be used to lead the expert system to the correct model in a computationally efficient manner.

Decisions in "expert" automatic classification systems such as the ones described here can be based on the shapes of residual or deviation plots obtained from the differences between computed and experimental data after a regression analysis. Such plots were discussed as tests for goodness of fit in Section II.E. According to the definitions in that section, for data following a model of the type in Equation 1, the deviation plot consists of a plot of dev_j/SD vs. x_j, where $dev_j = y_j(\text{meas}) - y_j(\text{calc})$. Values of dev_j/SD will have a random distribution around the zero abscissa (i.e., $dev_j = 0$) if the regression model is correct and if there are no systematic errors in the measurements. If the model incorrectly describes the data, the resulting deviation plot will be arranged in a distinct pattern. Scatter superimposed around this pattern reflects random noise in the measured response.

Actual noise-free "deviation patterns" for fits onto a given model can be computed by nonlinear regression analyses of noise-free simulated data sets representing the other models in the library. These computed deviation patterns can be compared with the shape of the deviation plot for the experimental data. Deviation plots are often numerically smoothed to facilitate such comparisons. The model with a deviation pattern closest to the shape of the experimental deviation plot is considered to have a good probability of being the correct choice. This model is used for the next regression analysis. By repeated application of this procedure, known as "deviation pattern recognition", the correct model is found if it is present in the library of models. Deviation pattern recognition originated in the research of Meites and co-workers and was described in an earlier review.[1] Meites has applied these methods to develop automated, computerized classification systems for determining the number of acidic protons in an unknown weak acid, for investigating the behavior of micelles from titration data, for finding the maximum coordination number of a complexed metal ion from electrochemical data,[1] and for elucidating mechanisms of electrode reactions from charge-time data for bulk controlled-potential electrolyses.[67] A few more recent applications of these classification methods are discussed in detail in the following sections.

B. Classification of Multiexponential Decay Data

First-order decomposition of a given species is often monitored in experiments designed to study luminescence decay, radioactive decay, and the kinetics of irreversible first-order chemical reactions. For mixtures of p components all undergoing first-order decay with lifetimes $\tau_j = 1/k_j$, the data are represented by a sum of exponentials:

$$I = \sum_j A_j \exp(-t/\tau_j); \qquad j = 1,\ldots,p \qquad (74)$$

where I is the measured intensity of the decaying species at a single energy or wavelength, and k_j is the first-order rate constant for decay of the jth component. Nonlinear regression analysis of I vs. t data can provide the 2p parameters A_j and τ_j, but a judgment must be made concerning the correct number of exponentials in the model. The problem is similar to the choice of the correct number of components for the multicomponent time-resolved fluorescence spectra discussed in Section IV.F.

A prototype automated method for analyzing multiexponential decay curves was developed based on deviation pattern recognition. The computer program sequentially fits models involving one, two, and three exponentials to the experimental decay data,[12] stopping when the correct model is found. The choice of the correct model is based upon predefined criteria of randomness in weighted, smoothed deviation plots. The computer program estimates initial values of regression parameters from separate linear regressions of sectionalized data sets. Nonlinear regression analyses were done with a modified steepest descent subroutine in the main classification program.

A subroutine containing the regression model in Equation 74 was constructed with logical statements to do sequential fits with p = 1, 2, and 3. The error sum in Equation 2 was minimized with $w_j = 1/I_j(\text{meas})$. This weighting factor is consistent with the dependence of random error in photon-counting experiments on the square root of the measured number of counts. After acquisition of the I vs. t data, the program estimates initial values of A_1 and τ_1 by a preliminary *linear* regression of log I vs. t. These initial values of the parameters are used to begin the first nonlinear regression onto Equation 74 with p = 1. Following this nonlinear regression, a weighted deviation plot of $[I_j(\text{meas}) - I_j(\text{calc})]/[\text{SD}\ \{I_j(\text{meas})\}^{1/2}]$ vs. t is constructed. A moving three point sum (D_s) was used to smooth the deviation plot to minimize the effect of noise, which may obscure any pattern present. Based on studies with simulated noisy data, a threshold representing the definition of a peak in the smoothed deviation plot was arbitrarily set at 3.75 (SD). Assuming that the model is correct and that

systematic error is absent, the probability obtained from the normal curve of error of one weighted deviation exceeding 1.25 (SD) is 0.21. Thus, the probability of one D_s exceeding 3.75 (SD) is $(0.21)^3 = 0.0095$, or a bit less than 1%. Absolute values of the moving sum D_s are now sequentially tested to see if any exceed the threshold value. If the threshold is not exceeded, the deviation plot is considered random, the $p = 1$ hypothesis is accepted, and the best values of A_1 and τ_1 are communicated to the user. However, if the threshold is exceeded by one or more D_s, the smoothed deviation plot is considered nonrandom and the $p = 1$ hypothesis is rejected.

Next, in preparation for a second nonlinear regression, the data are arbitrarily split into two parts along the time axis. Semilogarithmic linear regressions are done on each part to find four new initial parameters. A nonlinear regression of the full data set onto Equation 2 with $p = 2$ is then begun. After convergence, the threshold-testing procedure is repeated for the resulting smoothed deviation plot. If no new D_s exceed the threshold, the $p = 2$ hypothesis is accepted. If one or more D_s exceed the threshold, a third and final nonlinear regression with $p = 3$ is initiated. Initial parameters are again chosen automatically by linear regressions on the data set divided into three parts. The new smoothed deviation plot is used as above to test the $p = 3$ hypothesis.

Studies with simulated data containing noise approximating that in typical luminescence decay experiments on particulate materials were used to explore the limits of reliability of the classification program. Data representing one, two, or three exponential decays were correctly classified when individual successive lifetime ratios exceeded 2.3 (i.e., for 2 or 3 exponentials, τ_2/τ_1 and/or τ_3/τ_2 exceeded 2.3). The method was applied to luminescence decay data for different types of zeolites (molecular sieves) into which uranyl ions had been exchanged. Multiple exponential decays correspond to uranyl ions in different environments in the zeolite.[68] When data for uranyl in the zeolite sodium mordentite were analyzed by the automated classification program, the smoothed deviation plot from the $p = 1$ fit was clearly nonrandom (Figure 16) and was classified as such by the program. The smoothed deviation plot $p = 2$ was similar in shape to Figure 17. The fit was better, but the plot still appears nonrandom. Three of the D_s values exceeded the threshold. Figure 17 illustrates high-frequency systematic instrumental noise superimposed on the broad (low frequency) characteristic features expected from fitting a $p = 2$ model to data from a three-exponential system.[69] This was typical of all luminescence data investigated. Nevertheless, the subsequent $p = 3$ fit gave a smoothed deviation plot with no points exceeding the threshold, and the $p = 3$ hypothesis was accepted. The same conslusion was reached independently by the inorganic chemists who collected the data after visual inspection of the results of nonlinear regressions.[68] The parameters for the $p = 3$ fit were in good agreement with those reported previously.[12]

The program was unable to classify data from a uranyl/NaZSM-5 sample because of the troublesome high frequency

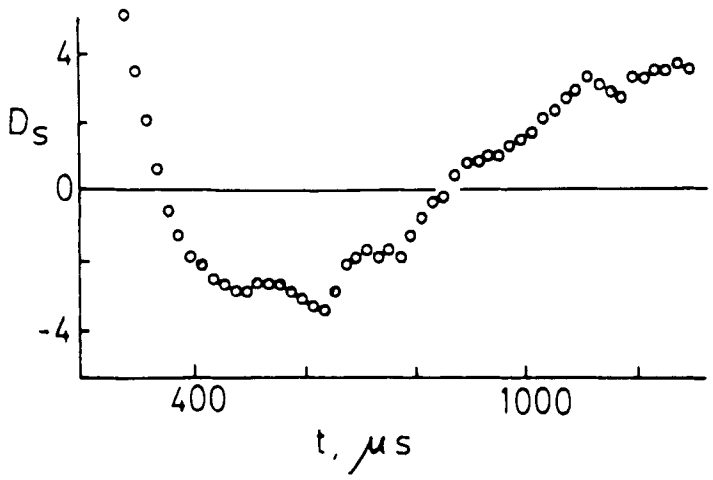

FIGURE 16. Smoothed deviation plot for luminescence decay of uranyl-Na mordenite sample regressed onto model for single exponential decay. (Reprinted from Brooks, M. Y. and Rusling, J. F., *Anal. Lett.*, 18, 2021, 1985. With permission. Copyright 1985, Marcel Dekker, Inc.)

noise illustrated in Figure 17. For good classification efficiency, systematic noise in the data needs to eliminated. With respect to the high-frequency noise level in the data used, the three-point moving smooth routine did not provide sufficient filtering.

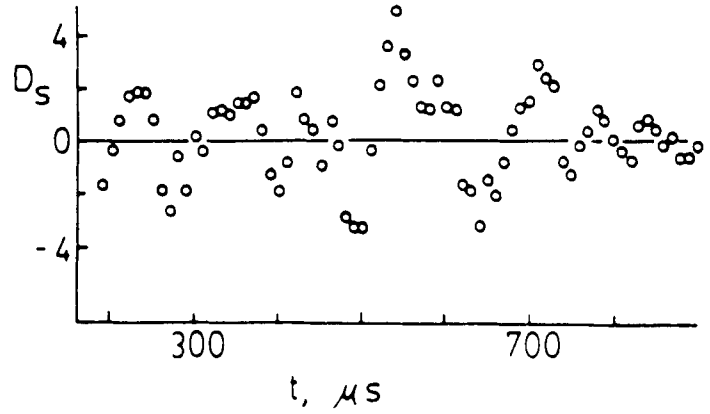

FIGURE 17. Smoothed deviation plot for luminescence decay of uranyl-NaZMS-5 sample regressed onto triple exponential model. The appearance of this plot reflects systematic high-frequency noise in the data. (Reprinted from Brooks, M. Y. and Rusling, J. F., *Anal. Lett.*, 18, 2021, 1985. With permission. Copyright 1985, Marcel Dekker, Inc.)

C. Statistical Comparison of Models with Different Numbers of Parameters

The program described above is an example of a linear classification scheme. In it, models are tested in a logical linear progression until the correct one is identified. The models are all of the same form, but the number of parameters is twice the number of components in the sample. Classification in this case was done entirely on the basis of deviation pattern recognition. As a check on the results, summary statistics could

also be used in such programs. However, the models in the exponential decay problem have different numbers of parameters. Thus, the individual regression analyses have different numbers of degrees of freedom, defined as the number of data points less the number of parameters. This must be accounted for when using a summary statistic to compare the applicability of two models. A statistical test that can be used in such situations employs the extra sum of squares principle.[70] This involves calculating the F ratio:

$$F(p_2 - p_1, h - p_2) = \frac{(S_1 - S_2)/(p_2 - p_1)}{S_2/(h - p_2)} \quad (75)$$

where S_1 and S_2 are the residual sums of squares (error sums) obtained from regression analyses of the same data onto the two models (cf. Equation 2), h is the number of data points, p_1 and p_2 now represent the numbers of parameters, and the subscripts refer to the specific models. To use Equation 75, model 2 should be a generalization of model 1, a condition fulfilled for the exponential decay problem. Equation 75 accounts for different numbers of degrees of freedom in the models being compared.

As an example of the use of Equation 75, we apply it to test the conclusions reached for luminescence data on uranyl-exchanged sodium mordenite discussed in the previous section. Weighted regression analyses of 55 pairs of I vs. t data onto the models with one, two, and three exponentials were done with a Marquardt program and the following error sums resulted: $S_1 = 1843$, $S_2 = 69.01$, and $S_3 = 61.95$. Applying Equation 75 to compare two- and three-exponential models gave $F(2,49) = 2.79$. From the F-tables, at the 90% confidence level, $F(2,49)_{90\%} = 3.19$, while at the 80% confidence level $F(2,49)_{80\%} = 2.42$. The experimental F falls between these values, indicating at least an 80% probability that the difference between S_3 and S_2 is statistically significant, i.e., $S_3 < S_2$ at the 80% confidence level. This confirms the conclusion made in the previous section based on deviation pattern recognition. Comparing the one- and three-exponential fits, we find $F(4,49) = 352$. Since $F(4,49)_{99.8\%} = 5.5$, we conclude that $S_3 < S_1$ with greater than 99.8% probability.

We see that deviation pattern recognition provides an automatic way of testing models. In some cases, alternative models will have different numbers of parameters causing the respective regression analyses to have different degrees of freedom. Deviation plots in conjunction with the extra sum of squares F-test described earlier provide techniques to reliably distinguish between such models.

We digress briefly here to discuss the practical significance of the number of parameters in a nonlinear regression model with respect to analyzing data. Many chemists still may hold the erroneous and simplistic view that a sufficient number of parameters will always lead to a better fit of the model to the data. This point was discussed by Meites,[1] who used the example of a seven-parameter polynomial equation which gave a poor fit to data for the potentiometric titration of potassium acetate with HCl. When the correct titration equation containing only four parameters was used, an excellent fit was obtained with a random deviation plot and a standard deviation of only ±0.2% in the concentration of the unknown acetate. Another example cited was an eight-parameter empirical equation having no basis in theory which gave only approximate fits to LSV curves for reductions of several metal ions in water. Rather unacceptable relative standard deviations of regression of about 2 to 3.3% and systematic errors in the computed currents were found with the empirical model.[71] In contrast, relative standard deviations better than about 0.6% and nearly random deviation plots have been achieved routinely for regressions of LSV data for reversible reductions of organic compounds in DMF onto the correct four-parameter digitally simulated model.[4] Many similar examples could be given, all demonstrating that increasing the number of parameters will not compensate for an incorrect model. Simply adding more parameters to an incorrect model will not make the model fit! On the other hand, including as many parameters as needed in a theoretically relevant model is not a limitation to a successful regression method so long as the parameters are not correlated and the data sets are large enough.

This discussion indicates that rigorous testing of models with different numbers of parameters, such as described in the exponential decay case, can be relied upon. For example, addition of the third exponential to the model for the uranyl-zeolite luminescence data discussed previously would not provide a good fit if the model was incorrect. This could be demonstrated, as implied above, by comparison to a six or more parameter fit using a grossly incorrect model. However, it is the nature of scientists to be skeptical. Many will not be convinced of these facts until they have firsthand experience with model testing using nonlinear regression analysis. This course of action is recommended to all skeptics.

D. Automated Classification of Steady-State Voltammograms

We have already seen that the shapes of steady-state voltammetric i-E curves depend on the electrode reaction mechanism which gives rise to them. Thus, Equation 10 describes fast (or reversible) electron transfer reactions, Equation 11 holds for two overlapped waves, Equation 19 describes the curve shape for an electrodimerization (EC2 reaction), and Equation 33 applies for moderately slow (or quasireversible) electron trasnsfer. Deviation pattern recognition was used as the basis for automatic classification of steady-state voltammetric curves as to the mechanisms of their electrode reactions.[25] Again, the main principle employed to construct the program was that nonrandom deviation plots have shapes which are generally characteristic of the chemical behavior governing the shapes of the response curves.

The automated mechanistic classification program was arbitrarily designed to begin with an initial fit to Equation 19, corresponding to the EC2 mechanism. Consider, for example, a nonlinear regression onto Equation 19 of noise-free steady-state voltammetric data computed for a reversible electron transfer reaction (Equation 10). The EC2 model is wrong, and the resulting "deviation pattern" has the shape of curve B in Figure 18. For the ten mechanistic classes in Table 4, deviation patterns for fits of simulated data onto the EC2 model were all of shape A or B (Figure 18). The classification program was constructed such that it "memorized" the shapes of the deviation patterns for all possible fitting situations and could make a decision based on the shape of the deviation plot found for a given set of experimental data. In this way, in conjunction with tests of the physical reasonableness of computed parameters, the program progressed toward an acceptable hypothesis.

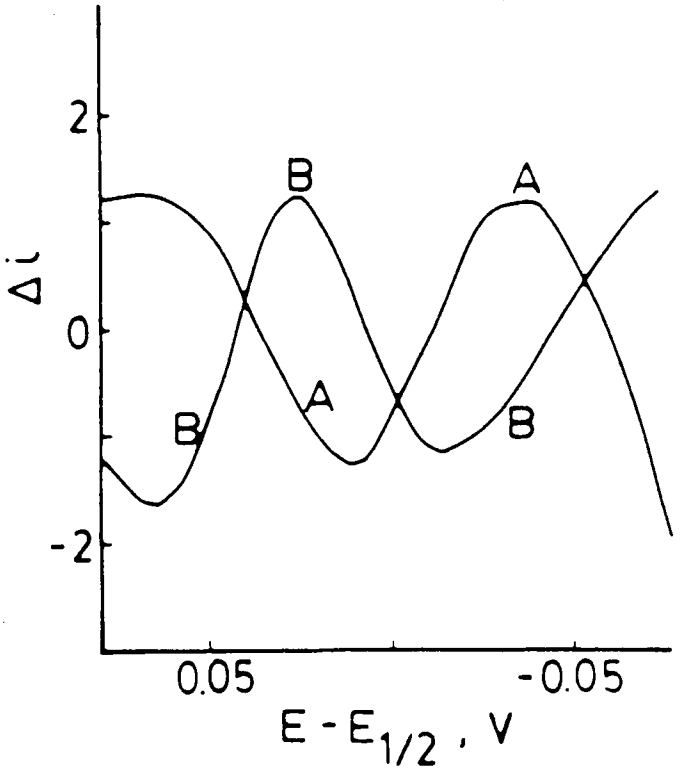

FIGURE 18. Type A and Type B theoretical deviation patterns obtained with simulated noise-free steady-state i-E data. (Reprinted from Rusling, J. F., *Anal. Chem.*, 55, 1713, 1983. With permission. Copyright 1983, American Chemical Society.)

Theoretical deviation patterns were used to construct a hierarchical classification tree (Figure 19) to guide efficient decision making within the program. As mentioned previously, the shapes of the deviation patterns from fits onto the EC2 model fell into three classes: a random plot confirming the EC2 mechanism, a "type A" plot suggesting DIFF-R, DIFF-I,

Table 4
Library of Models for Automated Classification of Steady-State Voltammograms

Class[a]	Electrode reaction scheme
EC2	O + e = R; 2R → Dimer
DIFF-R	O + e = R (reversible)
(CE)[b]	Z = O; O + e = R
(EC)[b]	O + e = R; R → P
DIFF-I	O + e → R
EC2A	O + e = R(ads); R(ads) → Dimer(ads)
D-M	$(O)_2$ + 2e = 2R
QR	O + e = R (quasireversible)
W2	Two overlapped waves; model for product adsorption
NO MECH	Model not included in library

[a] Symbols: E = electron transfer; C = first-order chemical step; C2 = second-order chemical step.
[b] Cannot be distinguished from diffusion controlled when chemical step is fast.

Reprinted from Rusling, J. F., *Trends Anal. Chem.*, 3, 91, 1984. With permission. Copyright 1984 Elsevier.

D-M, QR, or W2 classes (Table 4), or a "type B" plot suggesting the EC2 or QR class. The QR mechanism fell into either class, depending on the magnitude of the standard heterogeneous rate constant. Essential features of the theoretical deviation patterns in the form of peak polarity, i.e., positive or negative, and peak position were encoded in the program

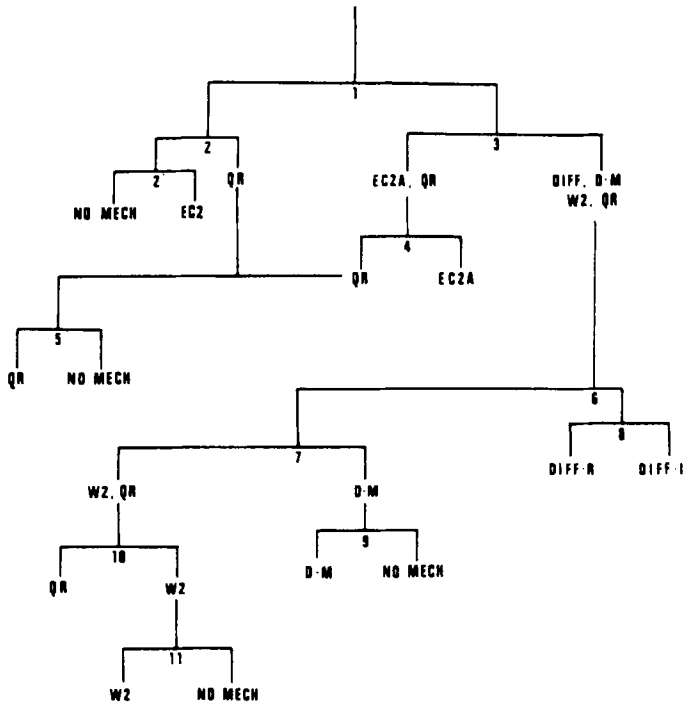

FIGURE 19. Hierarchical tree for mechanistic classification of one-electron, steady-state i-E data. (Reprinted from Rusling, J. F., *Anal. Chem.*, 55, 1713, 1983. With permission. Copyright 1983, American Chemical Society.)

as two binary numbers, one for positive peaks and one for negative peaks. This eliminates the need of storage space for the model library and facilitates comparison with smoothed experimental deviation plots. The program simply compares the values of base-ten representations of the binary numbers with the previously established ranges of these base-ten numbers for type A and type B plots. All nonrandom deviation patterns for data fit to any wrong model were of the type A or type B shape, further simplifying comparisons.

Following the initial fit of the data onto the EC2 model, the resulting deviation plot is tested for randomness. This test takes the form of a threshold analysis as described for the exponential decay program. If the deviation plot is random, the program terminates. If not, a test for type A or B shape is undertaken to decide which model to use for a second regression analysis. Each additional subgroup further along the branches of the classification tree was further subdivided by the shape of its deviation pattern. A model was chosen from each group for an initial regression analysis within that particular group. The adherence of the slope factor (S′) to its known theoretical value for the given temperature and mechanism was also monitored. Each branch point in the decision tree represents a decision based on either the shape of the deviation plot or the value of the parameter S′. The experimental data proceeds through the branches of the decision tree until an acceptable hypothesis is reached. This is indicated by a random deviation plot or a NO MECH classification.

The deliberations of the mechanistic classification programs can be illustrated with a steady-state voltammogram for the reduction of 0.66 m*M* ferriheme in 0.1 *M* NaOH.[25] Data were acquired by current-sampled polarography as 27 i-E pairs between 5 to 95% of the limiting current. The user provides an initial estimate of limiting current and the estimated standard error (SE) in the measured current. From these and the i-E data, the program estimates initial values of the parameters $E^{o'}$ and S′ and regresses the data onto the EC2 model. This yielded a type A deviation plot for the ferriheme data. The parameters computed are given in the second line of Table 5. Now decision 1 is reached. If the deviation plot had been random, the program would have terminated at this point. Since it was nonrandom, the computations are directed to decision 3. A test of the shape of the deviation plot indicates type A, and the program proceeds along the far right hand branch of the tree. This path requires a second regression analysis, this time onto the DIFF model. The results (Table 5) lead to decisions 7 (nonrandom deviation plot) and 9 (type A deviation plot), initiating a third regression analysis. For this fit onto the D-M model, the program finds that SE < 0.95 (SD), and dev_j/SE is used to construct the deviation plot. This feature is included to scale small deviations by an experimentally more realistic factor. It biases decisions toward models which provide better agreement with the data, even though small nonrandom deviations may still exist. For the ferriheme data, the final deviation plot is random and the program indicates the D-M model as the most likely hypothesis. Intermediate and final statistics and deviation plots are output for the user's inspection.

Table 5
Summary of Output from Automatic Classification of Current-Sampled Steady-State Voltammogram of 0.66 m*M* Ferriheme in 0.1 *M* NaOH[a]

NLR #	Model	$-E_{1/2}$(V)	S′(V)	i_l(μA)	SD(μA)	DP
0	Initial	0.713	0.0257	0.717	—	—
1	EC2	0.711	0.0317	0.807	0.0121	Type A
2	DIFF	0.718	0.0237	0.756	0.0089	Type A
3	D-M	0.736	0.0141	0.699	0.0037	Random[b]

[a] Standard error (SE) = 0.005 μA; S′ = RT/2F; E in Volts vs. SCE.
[b] SD < SE × 0.95, thus *dev*/SE was used for deviation plot (see text).

Reprinted from Rusling, J. F., *Trends Anal. Chem.*, 3, 91, 1984. With permission. Copyright 1984 Elsevier.

Random noise in steady-state voltammograms is essentially independent of the size of the current or is absolute (cf. Section II.C). Tests of the classification program with simulated data showed that for single-wave systems, 100% correct classifications could be expected if absolute random noise was below 0.85% of the limiting current. This is well within S/N capabilities of modern electrochemical instrumentation. Out of 44 sets of experimental data representing oxidations and reductions by rotating disk voltammetry, DC polarography, and normal pulse voltammetry, 36 sets were classified according to previously suggested mechanisms.[25] Eight DC polarograms for two reduction systems were found to exhibit subtle mechanistic nuances not previously recognized. The latter achievement is a direct result of the analytical power of deviation pattern recognition for distinguishing experimental behavior deviating even slightly from a regression model. The automated classification method classifies data conforming to simple mechanisms in the library without intervention of the user. It identifies the more complex systems with NO MECH classifications, indicating that the observed shape of the i-E curve is not included in the library of models.

Although automatic classification using deviation pattern recognition is one of the most exciting and potentially powerful applications of nonlinear regression analysis, it has not received a great deal of research attention. To this author's knowledge, the limited applications to date are summarized in this article and an earlier review.[1] This is unfortunate since information gathered by experts in a variety of fields could easily be used to construct such programs, thus allowing other chemists the benefit of high-quality, objective classification tools. Synergistic multitechnique approaches could be envisioned. With regard to the voltammetric classifications discussed earlier, suppose initial voltammograms were classified by such a program into class X, containing several closely related models. The program might then suggest experiments by a different technique, such as chronocoulometry or square-wave voltammetry, all within

the realm of classification and parameter estimation by the same program. Such a program could be designed to employ combinations of electrochemical, spectroelectrochemical, and other methods, much as an "expert" electrochemist might do intuitively. An advantage would be that these experiments could be suggested, completed, and interpreted automatically without requiring attention of the "expert" chemist. Furthermore, the program could be designed to access pertinent theoretical information and literature references concerning mechanisms of interest. Although, to this author's knowledge, the construction of such a program has not yet been attempted, it is certainly within the scope of present technology.

ACKNOWLEDGMENTS

The author is grateful to students, colleagues, and research associates named in joint publications for their assistance and enthusiasm. Much of the work described in this review would not have been possible without their help.The author is especially indebted to Dr. Johna Leddy, Artur Sucheta, and Azita Owlia for helpful comments concerning the evolving manuscript, and to Dr. Thomas Kumosinski for prepublication copies of References 57 and 58. Much of the work discussed in this article was generously supported by U.S. PHS Grant No. ES03154 awarded by the National Institute of Environmental Health Sciences, by a grant from the Petroleum Research Fund administered by the American Chemical Society, and by the University of Connecticut Research Foundation.

REFERENCES

1. **Meites, L.,** *Crit. Rev. Anal. Chem.*, 8, 1, 1979.
2. **Meites, L.,** *The General Nonlinear Regression Program CFT4A*, privately published, Potsdam, NY, 1983.
3. CET Research Group, *Nonlinear Least Squares Program NLLSQ*, privately published, Norman, OK.
4. **Arena, J. A. and Rusling, J. F.,** *Anal. Chem.*, 58, 1481, 1986.
5. **Arena, J. A. and Rusling, J. F.,** *J. Phys. Chem.*, 91, 3368, 1987.
6. **Connors, T. F., Arena, J. A., and Rusling, J. F.,** *J. Phys. Chem.*, 92, 2810, 1988.
7. **Johnson, J. K.,** *Numerical Methods in Chemistry*, Marcel Dekker, New York, 1980.
8. **Christian, S. D. and Tucker, E. E.,** *Am. Lab.*, p. 31, September 1982.
9. **Marquardt, D. W.,** *J. Soc. Ind. Appl. Math.*, 11, 431, 1963.
10. **Deming, S. N. and Morgan, S. L.,** *Anal. Chem.*, 45, 278A, 1973.
11. **Johnson, E. D., Weber, J. P., and Meites, L.,** *Anal. Chim. Acta*, 178, 263, 1985.
12. **Brooks, M. Y. and Rusling, J. F.,** *Anal. Lett.*, 18, 2021, 1985.
13. **Bard, Y.,** *Nonlinear Parameter Estimation*, Academic Press, New York, 1974.
14. **Kateman, G., Smith, H. C., and Meites, L.,** *Anal. Chim. Acta*, 152, 61, 1983.
15. **Brubaker, T. A., Tracy, R., and Pomernacki, C. L.,** *Anal. Chem.*, 50, 1017A, 1978; **Brubaker, T. A. and O'Keefe, K. R.,** *Anal. Chem.*, 5, 1385A, 1979.
16. **Meites, L. and Lampugnani, L.,** *Anal. Chem.*, 45, 1317, 1973.
17. **Shukla, S. S. and Rusling, J. F.,** *J. Phys. Chem.*, 89, 3353, 1985.
18. **Rusling, J. F. and Connors, T. F.,** *Anal. Chem.*, 55, 776, 1983.
19. **Kamau, G. N., Willis, W. S., and Rusling, J. F.,** *Anal. Chem.*, 57, 545, 1985.
20. **Sherwood, P. M. A.,** in *Practical Surface Analysis*, Briggs, D. and Seah, M. P., Eds., Wiley, New York, 1983, 445.
21. **Smith, D.,** Ph.D. thesis, University of North Carolina, Chapel Hill, NC, 1978.
22. **Kalyanasundaram, K. and Thomas, J. K.,** *J. Am. Chem. Soc.*, 99, 2039, 1977.
23. **Butler, J. N.,** *Ionic Equilibrium — A Mathematical Approach*, Addison-Wesley, Reading, MA, 1964, 79.
24. **Rusling, J. F.,** *J. Electroanal. Chem.*, 125, 447, 1981.
25. **Rusling, J. F.,** *Anal. Chem.*, 55, 1713, 1983; 55, 1719, 1983.
26. **Meites, L.,** *Anal. Lett.*, 15(A5), 507, 1982.
27. **Kateman, G., Smit, H. C., and Meites, L.,** *Anal. Chim. Acta*, 152, 61, 1983.
28. **Tanford, C.,** *Physical Chemistry of Macromolecules*, Wiley, New York, 1961, 526.
29. **Wyman, J.,** *Adv. Protein Chem.*, 19, 223, 1964.
30. **Owlia, A. and Rusling, J. F.,** *J. Electroanal. Chem.*, 234, 297, 1987.
31. **Lapidus, L. and Pinder, G. F.,** *Numerical Solution of Partial Differential Equations in Science and Engineering*, Wiley, New York, 1982.
32. **Joslin, T. and Pletcher, D.,** *J. Electroanal. Chem.*, 49, 171, 1974.
33. **Feldberg, S. W.,** *J. Electroanal. Chem.*, 127, 1, 1981.
34. **Ralston, A. and Meek, C. L., Eds.,** *Encyclopedia of Computer Science*, Petrocelli/Charter, New York, 1976.
35. **Shukla, S. S. and Rusling, J. F.,** *Anal. Chem.*, 56, 1347A,1984.
36. **Hamming, R. W.,** *Numerical Methods for Scientists and Engineers*, 2nd ed., McGraw-Hill, New York, 1973.
37. **Shukla, S. S. and Rusling, J. F.,** *Trends Anal. Chem.*, 4, 229, 1985.
38. **Bard, Y.,** *Nonlinear Parameter Estimation*, Academic Press, New York, 1974, 316.
39. **Rusling, J. F.,** *Anal. Chem.*, 56, 575, 1984.
40. **Connors, T. F., Owlia, A., and Rusling, J. F.,** *Anal. Chem.*, 57, 170, 1985.
41. **Carter, M. T., Kamau, G. N., and Rusling, J. F.,** *J. Electroanal. Chem.*, 170, 265, 1984.
42. **Fleischmann, M., Pons, S., Rolinson, D. R., and Schmidt, P. P.,** *Ultramicroelectrodes*, Datatech, North Carolina, 1987.
43. **Owlia, A. and Rusling, J. F.,** *Electroanalysis*, 1, 141, 1989.
44. **Adams, R. N.,** *Electrochemistry at Solid Electrodes*, Marcel Dekker, New York, 1969.
45. **Cabannis, G. E., Diamantis, A. A., Murphy, W. R., Linton, R. W., and Meyer, T. J.,** *J. Am. Chem. Soc.*, 107, 1845, 1985.
46. **Osteryoung, J. and O'Dea, J. J.,** in *Electroanalytical Chemistry*, Vol. 14, Bard, A. J., Ed., Marcel Dekker, New York, 1986, 209.
47. **O'Dea, J. J., Osteryoung, J., and Osteryoung, R. A.,** *J. Phys. Chem.*, 87, 3911, 1983.
48. **O'Dea, J. J., Osteryoung, J., and Lane, T.,** *J. Phys. Chem.*, 90, 2761, 1986.
49. **Anson, F. C.,** *Anal. Chem.*, 38, 54, 1966.
50. **Christie, J. H., Osteryoung, R. A., and Anson, F. C.,** *J. Electroanal. Chem.*, 13, 236, 1967.
51. **Anson, F. C.,** *Acc. Chem. Res.*, 8, 400, 1975.
52. **Murray, R. W.,** in *Physical Methods of Chemistry*, Part IIa, Weissberger, A., Ed., Wiley, New York, 1971, 591.
53. **Rusling, J. F., Brooks, M. Y., Scheer, B. J., Chou, T. T., and Shukla, S. S.,** *Anal. Chem.*, 58, 1942, 1986.
54. **Rusling, J. F. and Brooks, M. Y.,** *Anal. Chem.*, 56, 2147, 1984.

55. **Brooks, M. Y.,** Ph.D. thesis, University of Connecticut, Storrs, 1984.
56. **Meites, L. and Hussam, A.,** *Anal. Chim. Acta,* 204, 295, 1988.
57. **Farrell, H. M. and Kumosinski, T. F.,** *J. Ind. Microbiol.,* 3, 61, 1988.
58. **Kumosinski, T. F.,** *J. Agric. Food Chem.,* 36, 669, 1988.
59. **Rusling, J. F., Shi, C.-N., and Kumosinski, T. F.,** *Anal. Chem.,* 60, 1260, 1988.
60. **Owlia, A.,** Ph.D. thesis, University of Connecticut, Storrs, 1988.
61. **Knorr, F. J. and Harris, J. M.,** *Anal. Chem.,* 53, 272, 1981.
62. **Knorr, F. J., Thorsheim, H. R., and Harris, J. M.,** *Anal. Chem.,* 53, 821, 1981.
63. **Frans, S. D., McConnell, M. L., and Harris, J. M.,** *Anal. Chem.,* 57, 1552, 1985.
64. **Frans, S. D. and Harris, J. M.,** *Anal. Chem.,* 56, 466, 1984.
65. **Frans, S. D. and Harris, J. M.,** *Anal. Chem.,* 57, 1718, 1985.
66. **Dessy, R. E.,** *Anal. Chem.,* 56, 1200A, 1984.
67. **Meites, L. and Shia, G. A.,** in *Chemometrics,* Kowalski, B., Ed., American Chemical Society, Washington, D.C., 1977, 127.
68. **Suib, S. L., Kostapapas, A., and Psaras, D.,** *J. Am. Chem. Soc.,* 106, 1614, 1984.
69. **Demas, J. N.,** *Excited State Lifetime Measurements,* Academic Press, New York, 1983.
70. **Kinniburgh, D. G.,** *Environ. Sci. Technol.,* 20, 895, 1986
71. **Gutknecht, W. F. and Perone, S. P.,** *Anal. Chem.,* 42, 906, 1970.